POLYTECHNIC OF TURIN

Department of Electronics and Telecommunications

Master degree in

ELECTRONIC ENGINEERING

THESIS

Development of an optical amplifier in phosphate glass for LIDAR applications

Supervisors:

Prof. Davide Luca Janner

Dr. Nadia Giovanna Boetti

Author:

Simone Pagliariccio

Academic year 2018/2019

Contents

Introduction

This thesis reports on the experimental realization and characterization of a phosphate glass optical amplifier for LIDAR applications.
The work realized during this thesis is part of a project funded by NATO, whose name is C.A.L.I.B.E.R. (CompAct eye-safe LIdar source for AirBorne lasER scanning). The CALIBER project aims to implement a laser source in the perspective of its installation in a LIDAR (Light Detection and Ranging) system for monitoring sensitive environments.

The objective of the reported research activity is the fabrication and the optical characterization of an optical amplifier based on phosphate glasses, that are special glasses able to incorporate large quantities of laser-active rare earth ions (such Erbium (Er) and Ytterbium (Yb)), providing in this way an highly compact section of optical amplification, able to operate in the 'eye-safe' third telecommunication window (around 1550 nm).
The Er and Yb dopants simplify also the laser integration in a more complex system through the various choice of components available at reasonable commercial prices.

This thesis is structured in chapters. The first is dedicated to the presentation of CALIBER project, the second and the third provide an overview of the main theory concepts, such as LIDAR systems working principle, and the phosphate glass and optical fibers characteristics, focusing the analysis on the specifications of this research project. The fourth chapter shows the adopted method, from the glass fabrication and characterization to implementation in the amplifier set-up. Finally the fifth and the sixth chapter report the results and the conclusions.
All this thesis work was conducted in the applied photonics lab, called Photonext, that is located within the Links Foundation (previously Istituto Superiore Mario Boella).

CALIBER Project

1.1 Presentation

The work realized during this thesis is part of a project named C.A.L.I.B.E.R. (CompAct eye-safe LIdar source for AirBorne lasER scanning), a project funded by NATO in the 'Science for Peace and Security' program.
The project website is the following: *https://caliber-project.eu*.

Figure 1.1 - Logo of the CALIBER project [1]

CALIBER is a cooperative international project led by LINKS Foundation and comprises the following research institutions: Polytechnic of Turin, Ben Gurion University (Israel) and Tampere University of technology (Finland).

Figure 1.2 - CALIBER project partners [1]

1.2 Project

The security and protection of borders, sensitive infrastructures, and strategic sites is of paramount importance. Actually, border control is mainly realized by human patrols securing the perimeter, and various night vision sensors, is strongly limited in terms of continuous coverage and resolution. Moreover, the current monitoring involves high cost in terms of work force and equipment. Compared to other sensors, LIDAR systems have proved to be more effective and precise for remote sensing applications; their significant advantage over standard vision cameras consists in the ability to measure distances with high accuracy and build a three-dimensional (3D) map of the scanned area.

The goal of Caliber project is so to realize an innovative, compact and efficient laser source suitable for being mounted on unmanned air vehicles (UAVs). The drones, through a LIDAR system, will be able to monitor gas and oil platforms, maritime and power plants infrastructures and strategic sites, for security and borders protection.

Therefore the project aims to develop a miniaturized version of a laser signal source, not resorting to voluminous and heavy configurations as in the past.

The design started from the parallel implementation of a new seed laser, that will provide a pulsed signal at low power, and an optical waveguide amplifier to be mounted in a configuration called Master Oscillator Power Amplifier (MOPA), capable of emitting an output signal with high power and high spectral quality.

Furthermore, the source is designed to emit photons in the so-called eye-safe region of the electromagnetic spectrum at a wavelength of about 1550nm, to maintain a relative safety for the retina of the human eye. This aspect will allow the development of a device capable of operating at greater distances thanks to the high power and the characteristic of being eye-safe.

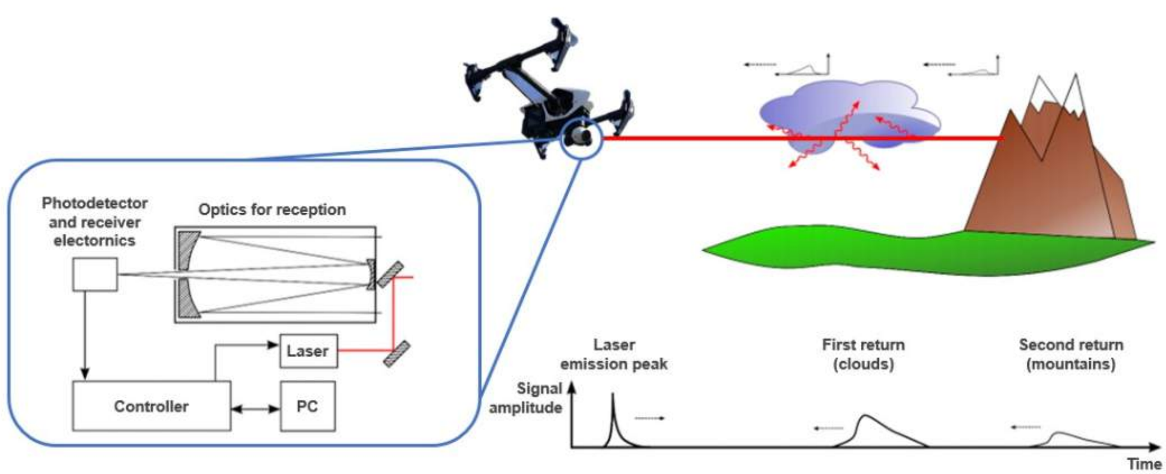

Figure 1.3 - LIDAR measurement principle [1]

1.3 Specifications

Therefore the project specifications are [1]:

- Develop an eye-safe microchip laser, the master oscillator, with high performance in terms of peak power and average power;
- Study and develop a new composition of phosphate glasses, to realize a compact optical amplifier operating at a wavelength of about 1550nm;
- Integrate the seed laser and the power amplifier into a compact MOPA source, that offers high power in an eye-safe range and with a competitive price.

LINKS Foundation and the Polytechnic of Turin are responsible for the design, development, and realization of the power amplifier.

The EDFA for LIDAR system

In this chapter an overview of the erbium doped fiber amplifier (EDFA) is exposed, analyzing it in the context of phosphate glasses in the perspective of its setting in a LIDAR system. The basic working principles are briefly recapped, respectively starting from the system level (LIDAR) towards the device level (phosphate glass fiber).

2.1 A LIDAR overview

LIDAR (Light Detection and Ranging) is an optical remote sensing technology, which measures properties of scattered light to find distance and/or other informations of a distant target. The prevalent method to determine distance to an object or surface is to use laser pulses. Similar to radar technology, which uses radio waves instead of light, the distance to an object is determined by measuring the time of flight (ToF), the time delay between transmission of a pulse and detection of the reflected signal (figure 2.1).

LIDAR is emerging as a cost-effective alternative to traditional surveying techniques for its ability to measure distances with high accuracy, and build a 3D map of the scanned area.

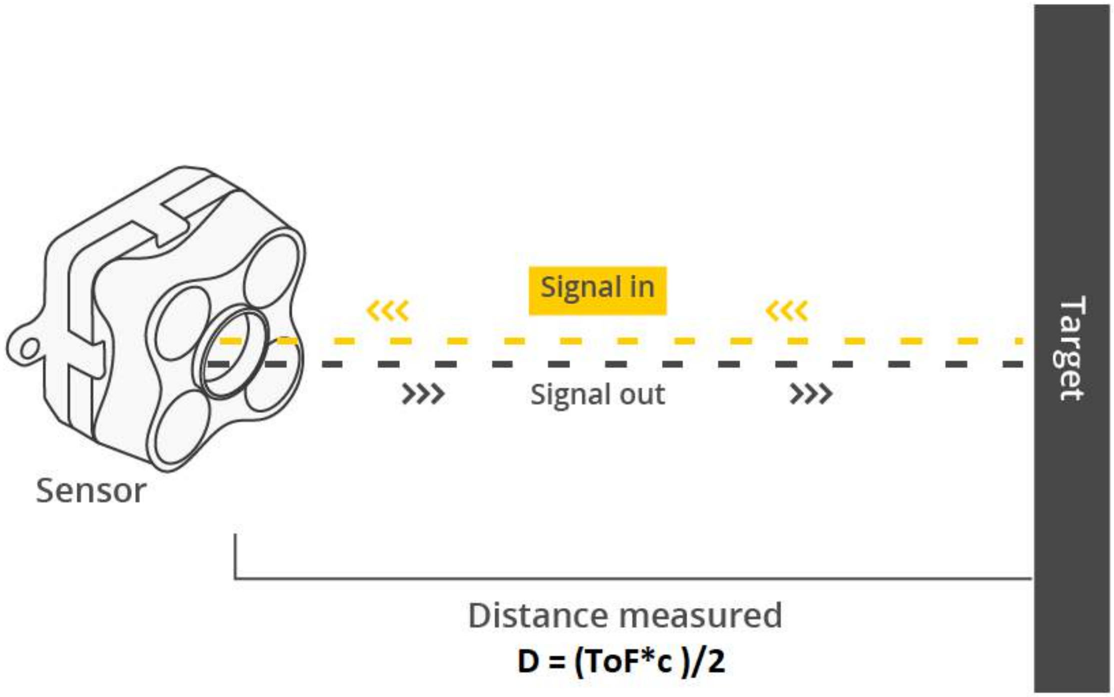

Figure 2.1 - LIDAR sensor working principle [2]

As showed in the image 2.1, LIDAR principle is based on the calculation of the distance between the LIDAR sensor and an object, through the knowledge of the speed of light (c), and the time delay between the pulse emission and its back-scattered detection.
The main steps are then:

- emitting a laser pulse (the sensor in the image 2.1 is also a pulse source),
- detecting with sensors the back-scattered laser light back to the LIDAR source,
- measuring the time laser travelled,
- calculating the distance from source with the formula above.

Repeating this process a million times ends up by producing a complex map of the surveyed area [3].

2.1.1 LIDAR types

In general, LIDAR typologies can be classified in 2 categories: terrestrial and air-borne LIDARs. There are two main types of terrestrial LIDARs: mobile and static [4]. In the case of mobile acquisition, the LIDAR system is mounted on a moving vehicle. In the case of static acquisition, the LIDAR system is typically mounted on a tripod or stationary device. The air-borne is similairly splitted in topographic and bathymetric; while the topographic is suitable for surface models, the bathymetric exploits a particular water penetrating acquisition system (figure 2.2).

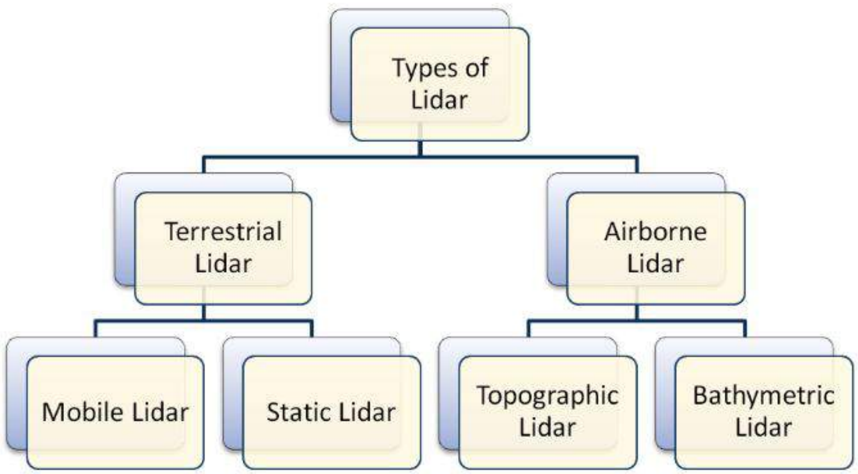

Figure 2.2 - LIDAR types classification[4]

The terrestrial ones (figure 2.3) are used for close-range high-accuracy applications, such as: bridge and dam monitoring, architectural restoration, and erosion mapping. They use an infrared or green wavelength laser, that emits pulses at rates up to 1000 Hz, and can map objects from about 1 meter up to 1000 meters away. Despite the accuracy of individual points can be affected by: atmospheric conditions, distance to the target, angle of incidence of the laser pulse upon the target, and the reflectivity of the target surface, the ground-based LIDARs can reach accuracies on the order of millimeters to a few centimeters.

Terrestrial LIDARs can be classified through different criteria, such as the operational range (short range up to 100m, medium range up to 250m, or long range up to 1km), or the employed scanning system.

Scanning methods can be:

- panoramic, that rotate 360 degrees around the mounting axis and scan 180 degrees vertically to provide seamless, and total coverage of the surroundings
- single axis, that rotate 360 degrees, but are limited to a 50-60 vertical swath
- camera, that point in a fixed direction with limited angular range both horizontally and vertically.

Figure 2.3 - Example of a terrestrial static LIDAR system [4]

2.1.2 Air-borne LIDAR type and specifications

The Air-borne LIDARs are installed in either a fixed-wing aircraft, or helicopters.
They emits an infrared laser light toward the ground, that returns to the moving airborne LIDAR sensor; they are capable of operating over a wide range of altitudes, to accommodate project-specific needs for accuracy, and broad area coverage.
As it was mentioned, there are 2 types of air-borne sensors: bathymetric and topographic sensors.
The first ones, applied for survey of the land-water interface, consist in an airborne acquisition that is water penetrating, collecting simultaneously elevation and water depth. With a bathymetric LIDAR survey, the infrared light (traditional laser system) is reflected back to the aircraft from the land and water surface, while the additional green laser travels through the water column. Analysis of the two distinct pulses are used to establish water depths and shoreline elevations. Bathymetric information is very important near coastlines, in harbors, and near shores and banks. Bathymetric information is also used to locate objects on the ocean floor.
The topographic LIDARs (CALIBER project ones) instead can be used to derive surface models for use in many applications, such as: forestry, hydrology, geomorphology, urban planning, landscape ecology, coastal engineering, survey assessments, and volumetric calculations.

In general, a LIDAR (figure 2.4) is composed of these fundamental submodules:

- a light emitter
- optics for the scanning process
- a photodetector
- a receiver electronics, that includes surely also a navigation and positioning system, since it is crucial to determine the absolute position and orientation of the sensor to make sure data captured are useable data, expecially in mobile LIDARs (such as Air-borne ones).

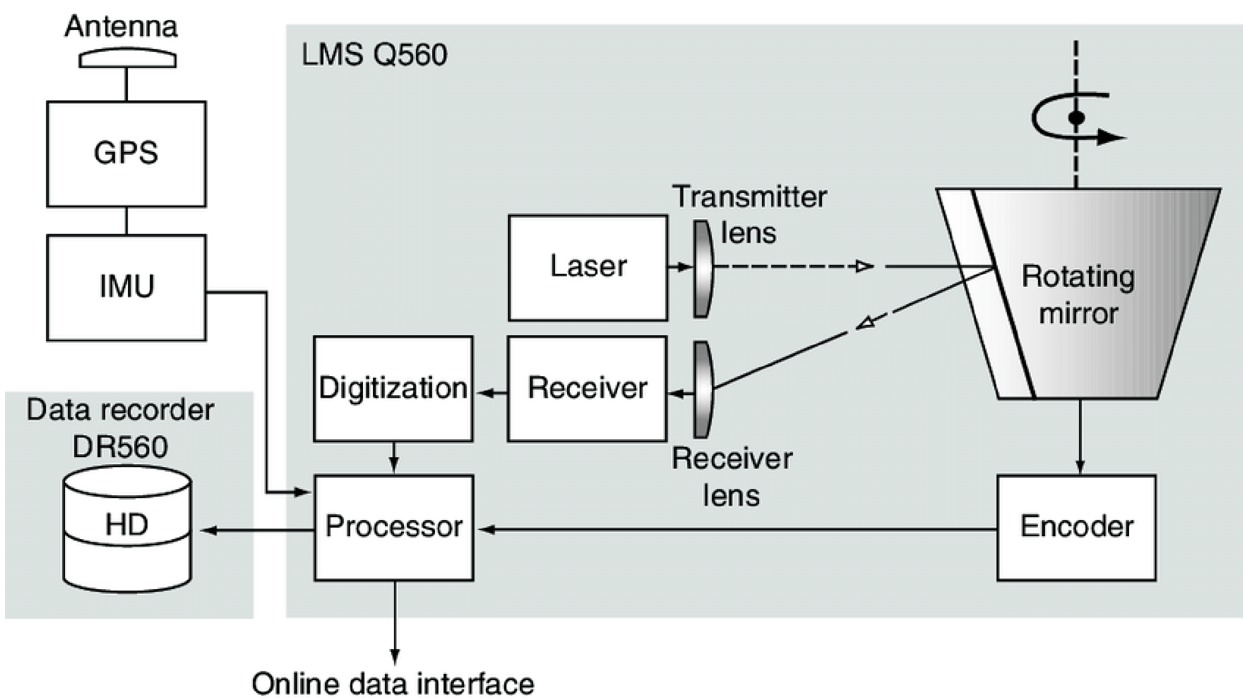

Figure 2.4 - An example of the Riegl LMS-Q560 scheme, an air-borne LIDAR laser scanning [5]

2.1.3 Source specifications

Among the LIDAR submodules, the CALIBER design focuses on the laser source, that itself contributes to overall system performance. In fact the laser beam quality and divergence, for example, is responsible for the lateral resolution of mapping lidars, while short pulse duration and low timing jitter are responsible for the longitudinal accuracy. Pulse energy is the key parameter to attain long ranges, while high pulse repetition rates allow faster scanning and high data throughput. [6]
An air-borne LIDAR source then permits an huge design freedom in the choice, for instance of:

- the laser operating principle: pulsed or continuous (CW). The pulsed ones, most commonly used for ranging applications, determine the target distance by recording the time taken by the transmitted pulse to reach the target and return back (at the speed of light). The continuous lasers on the contrary transmit a continuous signal, and performing a modulation carry out the distance measuring the travel time, that is directly proportional to the phase difference between the received and the transmitted sinusoidal signal.

- the operating wavelength: near-infrared, blue, or green. While the green wavelenghts penetrating the water, can be used for bathymetric sensors, the near-infrared wavelengths are used most by air-borne terrestrial lidar systems.

- laser system characteristics: power (the pulse energy is around 100μJ), pulse repetition frequency (from 1kHz up to 200kHz), scanning pattern (zig-zag, parallel, or elliptical) and footprint size.

- number of returns: single or multiple return, and waveform resolving. First return LIDARs measure the distance to the first target encountered by the pulse, two-stop LIDAR instead measure the distance to the first and last targets encountered, otherwise a multi-stop LIDAR measures the distances to multiple targets encountered by the pulse (in general the targets number is lower than 6). [7].

Among these typologies, high-peak-power pulsed solid-state lasers have been used in LIDAR applications for decades. Their size, weight, cost, power consumption, liquid cooling, sensitivity to shock and vibrations, and harsh environments have limited their diffusion in mobile, airborne, and space LIDAR applications.
Fortunately, the eye-safe lasers advent has permitted high-performance compact LIDAR solutions meant for civil and commercial applications (figure 2.5). In particular among eye-safe wavelengths, IR lasers emitting around 1.5 μm are often the choice when solid bodies need to be detected as in topography mapping and obstacle avoidance. In fact, the atmosphere is very transparent, and detectors are very efficient at 1.5μm.
The CALIBER project, facing those limitations and exploiting the eye-safe lasers emerging popularity, requires (as specified in the previous chapter) an infrared pulsed laser source solution suitable for topographic applications that, adopting a Master oscillator power amplifier (MOPA) configuration, tries to maximize the compactness achieving a proper laser quality.

Figure 2.5 - A YellowScan's LIDAR very accurate sensor, an example of compact solution of 1.6kg with 100x150x140(mm) size for UAVs [8]

2.2 Power scaling and MOPA approach

One of the main challenge, that the laser industries often face, is the power scaling.
The power scaling is rigorously defined as a well-defined systematic scaling procedure, which makes it possible to increase substantially and repeatedly the laser output power without:

- spoiling other essential performance parameters, such as the beam quality.
- relying on arbitrarily improved system components, (e.g. pump sources with arbitrarily high brightness)
- driving one component towards harsh conditions, such as excessive peak temperatures, damaging optical intensity levels.

Among the many solutions that achieve correctly this scaling, the MOPA configuration has proved to be one of the most popular approaches for amplification, preserving the beam main properties.
In this section at first some power scaling solutions are briefly exposed, then focusing more on the appropriate solution for the CALIBER project, the MOPA configuration characteristics are explained. [9]

2.2.1 Power scaling solutions

The conceptually simplest method to achieve power scaling is the beam combining. The beam combining is an effective solution, consisting in the flanking of collimated beams of lasers in independent execution, obtaining in such a way nearly unlimited amounts of output power, by simply combining the required number of lasers. So, even if the combined power increases in proportion to the number of lasers, the beam quality of the combined output decreases, because the beam area increases while the beam divergence remains constant, and the radiance (the optical power per unit area and solid angle) will at most stay at the level of a single laser. The beam quality is then in the beam combining technique a parameter to keep under control.
The beam combining type depends on the lasers quantity and quality; for instance for just two beams, having well-defined polarization states, a simple polarizer (e.g. a polarizing cube) could be sufficient (exploiting the so called polarization beam combining), but this method cannot be repeated, because it leads to an unpolarized beam. In the same way for different wavelenghts beams, it's performed a spectral beam combining (simply with a prism for instance), otherwise a coherent beam combining can be exploited with ordinary beam splitters for single frequency lasers with stable phase and polarized beams, or with optical feedback techniques for multi-mode lasers. [9]

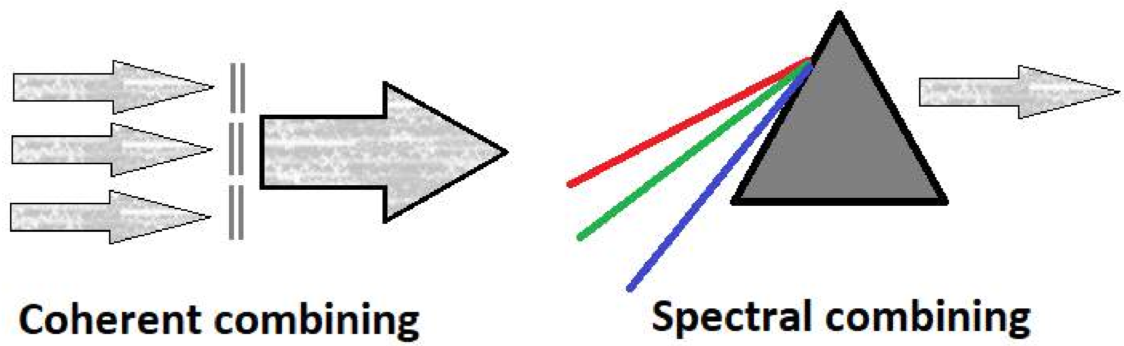

Figure 2.6 - Beam combining working principle

The image 2.6 shows the basic working principle of the coherent beam combining (CBC) and of an incoherent method, the spectral beam combining (SBC).
While in the first technique the outputs of the laser emitters, to be combined, are positioned side by side, forming a single spatially coherent larger aperture, in the SBC many optical beams, operating at a specific wavelength and directed at different angles, overlap spatially on a simple prism.

The power scaling can be simply faced, through a single high power laser properly designed. However, some laser types aren't suitable for true power scaling, for example: simple end-pumped or side-pumped rod lasers exhibit increasingly severe thermal effects with the pump power increase.
Actually, a type of laser resistant to negative thermal effects is the disk laser one. Disk lasers are special geometry solid-state lasers with a longitudinal heat flow (figure 2.7). With them power scaling is possible within a large range of output powers, because increasing the mode area in the gain medium (the thin disk) in proportion to the pump and output power, the maximum temperature excursion in the disk is not significantly increased: the cooled area increases in proportion to the power.
Therefore, the output power can be increased until effects related to mechanical stress in the disk or amplified spontaneous emission (ASE) in the transverse direction will eventually limit the performances.
Alternative solutions for power scaling are slab-lasers, where similairly to thin-disk lasers, the cooled area of the laser slab is scaled up for higher powers, so that the temperature rise, temperature gradient and induced stress do not have to be increased for higher powers. An other intermediate scaling method consists in the number of laser heads increase, using a single periodic laser resonator that does not spoil the beam quality.

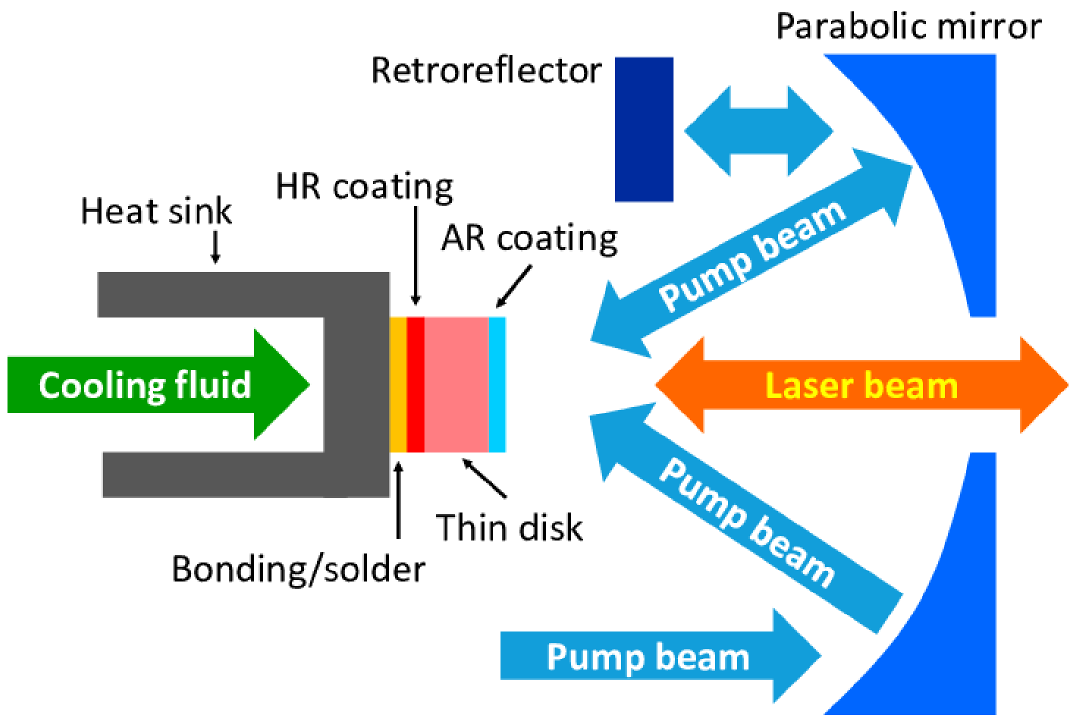

Figure 2.7 - Disk-laser working principle [10]

As it was said, beam combining techniques and thin disk lasers present theirself as effective power scaling solutions, that with the pump power increase still face performances constraints, such as beam quality and negative thermal effects. However as it was anticipated, the most strong method, against the power scaling challenge, is the MOPA configuration technique, whose architecture that splits the source laser from the power amplifier, permits easily to reach the required performances, such as beam quality etc.

2.2.2 A MOPA overview

A MOPA is a configuration consisting of: a master laser (or seed laser), and an optical amplifier to boost the output power (figure 2.8).
The optical intensities are lower in an amplifier, compared with the intracavity intensities in a laser.

Although a MOPA configuration is in principle more complex than a laser which directly produces the required output power, it can be advantageous.

- At first this configuration, thanks the performance aspects decoupling from the generation of high powers, permits extra flexibility in the reach of the required performances (linewidth, wavelength tuning range, beam quality, or pulse duration).
- The MOPA architecture avoids also the presence of additional optical components, such as wavelength tuning elements and modulation elements in a high-power laser resonator;

these elements can be placed inside the oscillator, in order to not have to withstand high optical intensities, and not spoiling the power efficiency etc..

However, the MOPA approach presents many disadvantages, such as: higher setup complexity, lower wall plug efficiency, higher resulting laser noise, and sensitivity to back reflections (often cured by placing a Faraday isolator behind the amplifier). For MOPA architectures adopted with pulsed laser sources: if a pulse from the seed laser extracts a significant fraction of the stored energy by the amplifier (used as reservoir), the amplifier gain drops during the pulse, since the effect of gain saturation is relevant. This can lead to a deformation of the temporal pulse shape. Consequently in some cases, the pulse shape from the seed source is tailored, so as to obtain the desired pulse shape after amplification. [9]

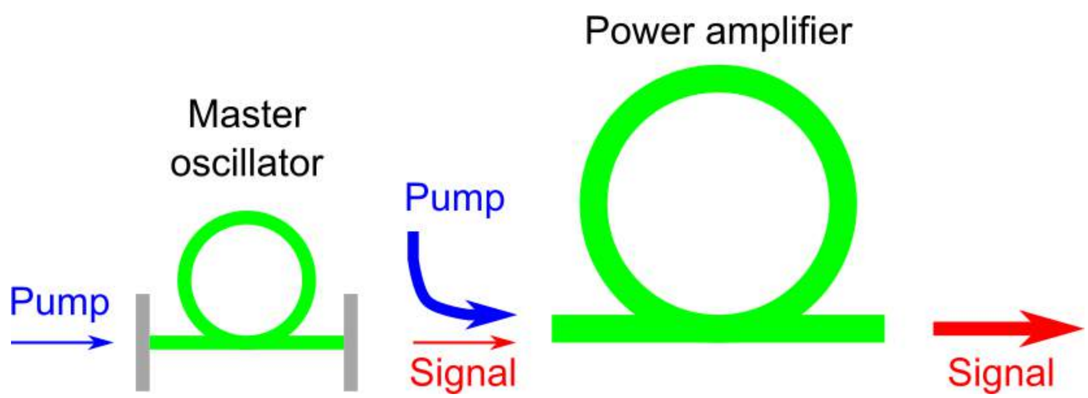

Figure 2.8 - MOPA General configuration scheme [11]

A MOPA special and very performant case, suitable expecially in a whole fibers connected system, is the MOPA configuration, where the power amplifier is a fiber device (as the one implemented in this thesis work).

2.2.3 MOFA and fiber amplifiers

The MOFA term (Master Oscillator Fiber Amplifier) refers to a MOPA configuration, where the power amplifier is a fiber device.
The fiber amplifier is an optical amplifier, whose gain medium is an optical fiber.
The use of a glass material for the optical amplifier shows the advantage, over the other types of materials, of combining: chemical stability, excellent homogeneity, good thermo-mechanical properties and a viscosity–temperature relationship that allows for shaping the waveguide into the form of optical fibers or rods. Moreover, glass displays a wide flexibility of the chemical composition and doping, allowing the preparation of multi-component glasses with properties that can be customized to meet the needs of the different applications.

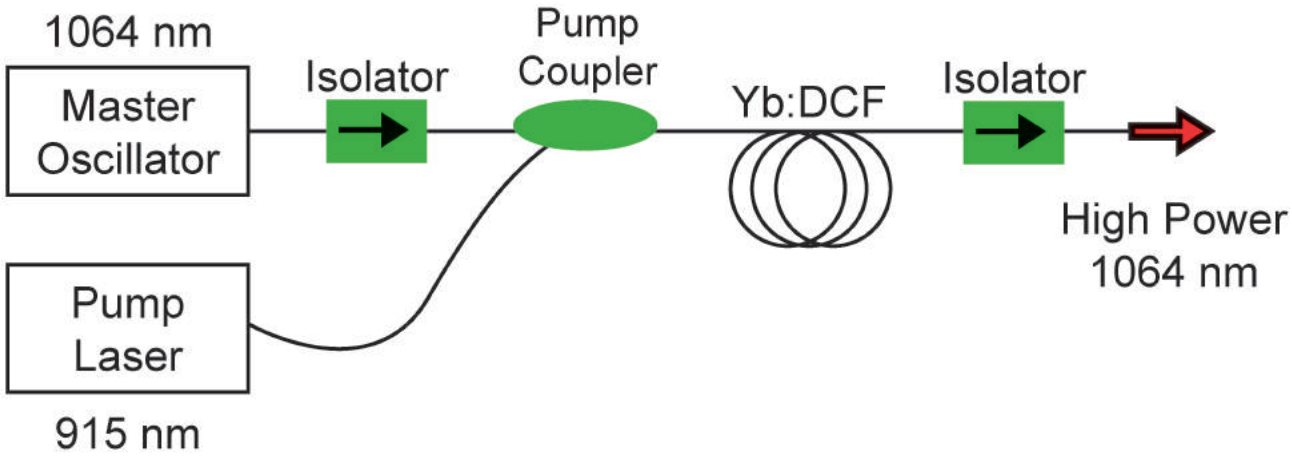

Figure 2.9 - Schematic of a MOFA emitting at 1064nm [12]

The image 2.9 sketches a MOFA simple scheme for a 1064nm signal amplification, whose fiber amplifier is an Yb doped fiber, pumped with a 915nm laser.
The MOFA method exhibit many advantages, such as:

- high power efficiency considering the high output power,
- high beam quality,
- higher gain than bulk amplifiers,
- and finally a relatively simple implementation of the cooling system.

However, the use of fibers also has disadvantages, such as: high back reflections sensitivity due to its high gain, high effort to reach high peak powers and pulse energies for fiber non linearities, stimulated Brillouin scattering (nonlinear scattering effect involving acoustic phonons in a transparent medium) in single frequency systems, and an often undefined and unstable polarization state.

2.2.4 CALIBER project MOFA configuration

The MOFA approach for the CALIBER project adopts a SESAM Q-switched microchip seed laser, and a an Yb-Er co-doped power amplifier; its configuration, including a 1550nm seed laser, a 980nm pump laser, and the optical amplifier, is depicted with its specifications in figure 2.10.

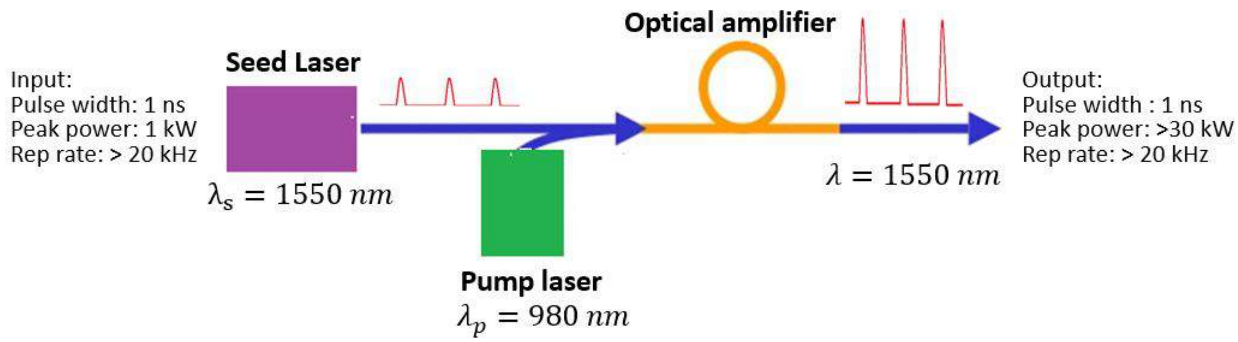

Figure 2.10 - Schematic of the CALIBER MOPA configuration [13]

The seed laser is a pulsed Q-switched microchip one. Pulsed Q-switched microchip lasers are highly compact and rugged laser sources, capable of producing energetic pulses with multi-kW peak power. They consist of a thin piece of laser gain material (crystal or glass), which is optically contacted to a saturable absorber (SESAM) that is used for initiating the pulsed operation. The saturable absorber can be made of doped glass, crystal, or semiconductor material. The gain element and the saturable absorber will form a monolithic structure, with plane-plane cavity geometry. The necessary laser mirrors are deposited directly on the cavity surfaces, making the laser free of cavity alignment. A laser operation in plane-plane type resonator is typically stabilized by a thermal lens. The laser output parameters, such as pulse width, pulse energy, pulse repetition rate, and spectrum are dependent on the combination of the gain material, saturable absorber, mode diameter and the laser coatings.
For the CALIBER project erbium-doped phosphate glass gain material (λ = 1535 nm), 976 nm diode pumping and SESAMs were used. The SESAMs consist of a distributed Bragg reflector (DBR) and a quantum well (QW)-based absorber section. [13]
Here in figure 2.11 the seed structure is depicted.

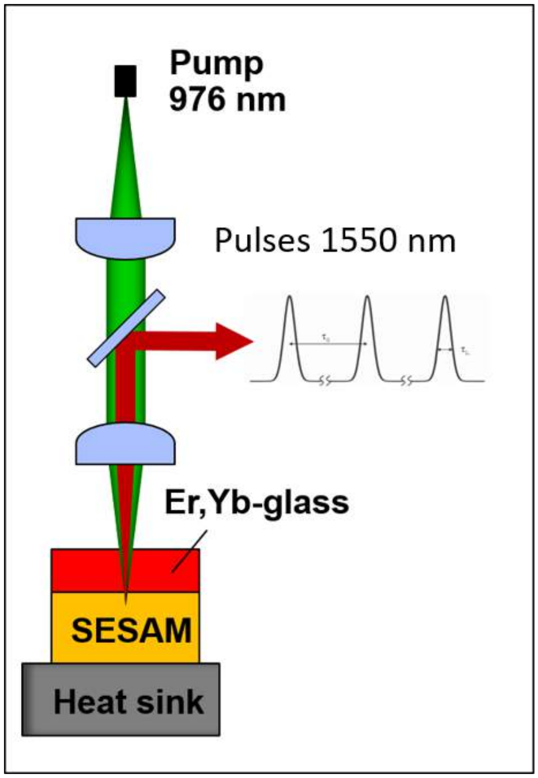

Figure 2.11 - CALIBER seed laser structure [13]

Continuing the CALIBER project MOPA analysis, the requests of a high degree of compactness at high performance and low cost, have obviously conditioned the selection of the optical amplifier too, whose choice fell on an Yb-Er co-doped glass-based waveguide.
A doped active fiber can be achievable through different glasses, able to host the rare earth active ions (such as Er and Yb). Among them it was proved, that phosphate glasses, thanks their outstanding solubility of laser active ions, provide the best performance in terms of optical amplification section. [9]

2.3 Phosphate glasses and optical amplification

This section tries to give a brief explanation at first of the phosphate glasses characteristics, and then of the optical amplification phenomenum. Each subject is before presented in general, and subsequently described in reference to the CALIBER project requirements.

2.3.1 Phosphate glasses characteristics

In general, in photonics glass materials have a real important role thanks their homogeneity, chemical stability, thermo-mechanical properties, viscosity temperature relationship (key component for fiber drawing), and finally (more important for this thesis work) great doping flexibility, that suggest a controlled engineerization.
In particular, a glass material is an amorphous solid, obtained from liquid state solidification preventing its crystallization. It differs from crystalline solid for the absence of order at long radius, that it's still mantained anyway at short and medium radius, as depicted in figure 2.12. [14]

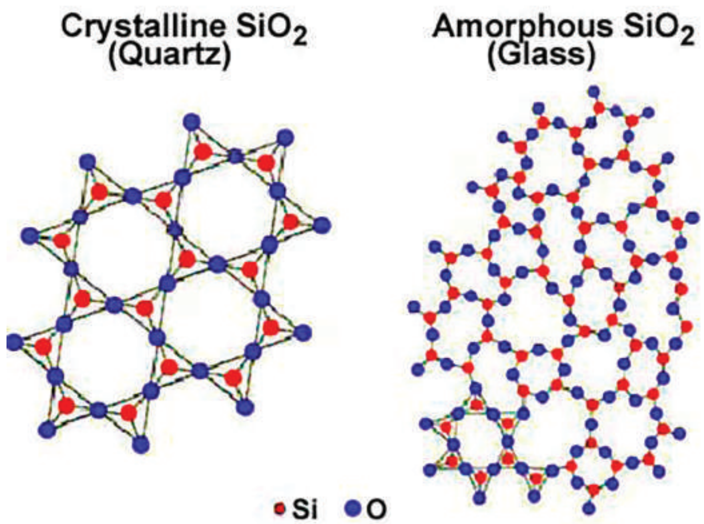

Figure 2.12 - SiO_2 quartz form on the left, glass form on the right[15]

In the case of inorganic materials a glass can be realized in practice mainly by substances belonging to the group of alides, chalcogenides and oxides as SiO_2, P_2O_5, B_2O_3, that for their role to generate the 3D randomic lattice are called lattice trainers. In the glass synthetization other substances that, causing the properties modification, partecipate to the process are lattice modifiers, such as: alkaline earth oxides, zinc oxides and alkaline oxides, that diffuse easily in the material thanks their weaker bonds. Their aim consists in the modification of the physical and chemical properties, (as fusion and lavoration caractheristic temperatures, refractive index ecc..). Other oxides as Al_2O_3, called intermediares, don't form the glass structure alone, but

partecipate in the amourphous network formation.
So, thanks the great flexibility of the glass in terms of chemical composition, is possible without a specific stoichiometry, realizing a material with certain requested characteristics as doping ions of rare earths.

Among the various glass families the one chosen for this thesis application is the phosphate glass family. A soft glasses family discovered with the laser advent in the 60s, devoted mainly on the production of compact laser devices (picture 2.13). The choice of these glasses for the CALIBER project was deemed more appropriate, thanks their effective skill of having very high solubility of laser-active rare earth ions, about 10 times higher than the solubility in silica-based glasses (most commercial ones).
These glasses permit then a greater doping concentration, so basically smaller dimensions for equal doping. They allow also an huge cross-section emission of rare earths in the inside, and a very temperature stable refractive index. Phosphate glasses for these reasons prove to be suitable for high power devices.[16]
Their realization is performed through P_2O_5, the lattice former that form the fundamental PO_4 structure. The so obtained glass is extremely reactive and hygroscopic, and this could be dangerous for the whole amplifier system, since the water acting as a lattice modifier, besides influencing badly mechanically, can also work as extinguishing centers of excited states. So the water must be managed to be reduced at minimum in the process. Lattice modifiers as alkaline, alkaline-earthy elements, or transiction metals can increase the glass stability and durability.
From a thermic point of view, the glass characteristics are lower: either since they present a lower melting temperature (1000-1200 C) than silica glasses (1600-1800 C), either since the glass transiction temperature is lower. The lower process temperatures favor greater simplicity of production, but suggests an high thermal degradation under high power operation (consequence of their lower thermal conductivity compared to silica glasses). This is the biggest limiting factor, that mantains phosphate glasses far away from achieving the same competitiveness level of silica glasses in the market of laser glasses.
The phosphate glass fibers are also more fragile, so they request more attention in the manipolation.
About this, the research team supported by this thesis has developed customized novel phosphate glasses, able to combine high RE ions solubility, highpower handling, enhanced thermal shock resistance, good thermal stability, suitability for fiber drawing, (since the fiber realization is performed with a 'drawing tower' instrument).

Figure 2.13 - An example Er^{3+}, Yb^{3+} doped phosphate glass [17]

2.3.2 Optical amplification

In an optical fiber, as it was already said, the light amplification can be performed thanks to a strong light material interaction. More specifically, the 'materials' that accomplish this interaction are the active ions Er^{3+} and Yb^{3+}, as doping elements, belonging to rare earth (lanthanides). It was observed that the trivalent ions, derived from atoms of elements belonging to the group of lanthanides, show strong phenomena of interaction with light when placed inside a glassy material. This is due to their particular electronic structure: with the partially completed orbital 4f, protected by the more external orbitals $5s^2$ and $5p^6$ (so less influenced by the external environment). This protection improves the optical amplifier performance, permitting longer light phenomena lifetime and narrower emission bands.
The spectroscopic processes of the active ions in a glassy host material are very similar to the phenomena observed in free ions, and are exposed in the following figure 2.14 with respect to the rare earths system used in this project.

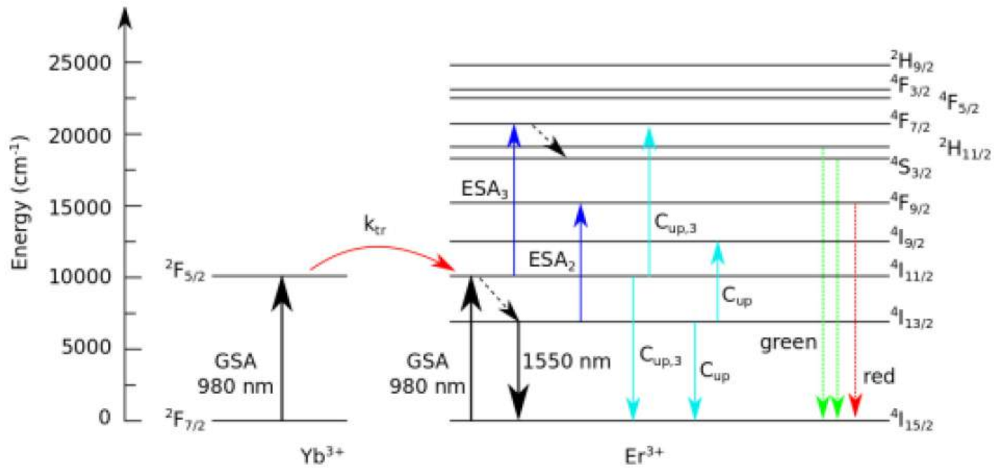

Figure 2.14 - Yb^{3+} and Er^{3+} Energetic levels and transitions [18]

The picture 2.14 exposes the fundamental processes of interaction between electrons and photons. In the image respectively, the Er^{3+} and Yb^{3+} energetic levels are represented by horizontal lines. The continuous, black upwards arrows represent the absorption mechanism, instead the downward arrows indicate stimulated emission phenomenum, where a photon is emitted with an energy equal to the energy difference between the levels. The dashed black arrows represent the not-radiative transitions, instead the dark blue and the light blue arrows identify respectively excited states absorption (ESA) and up-conversion phenomena.
Emissions in visible green and in visible red are highlighted with the reference color.
While the ytterbium ion system presents only the energy absorption mechanism between the levels $F^2_{7/2}$ and $F^2_{5/2}$, and the energy transfer between $F^2_{5/2}$ and $I^4_{11/2}$ levels to an adjacent ion Er^{3+} (continuous red arrow), the erbium ion system has more energy levels and various transitions between them. The main radiative erbium transaction takes place between levels $I^4_{13/2}$ and $I^4_{15/2}$, and is indicated by a black arrow pointing downwards. [19]

For this thesis project energy levels models can be simplified (figure 2.15), considering just the more relevant phenomena of optical amplification inside the phosphate glasses:

- The ESA_3, up-conversion 3 and consequently the green and red emission processes are negliglible, since the third energetic level ($I^4_{11/2}$) is subjected to a fast depopulation, thanks the extreme rapide energetic decay between the levels $I^4_{15/2}$ and $I^4_{13/2}$ of the ions Er^{3+}
- The ESA_2 process is negligible for low and medium power lasers[20].

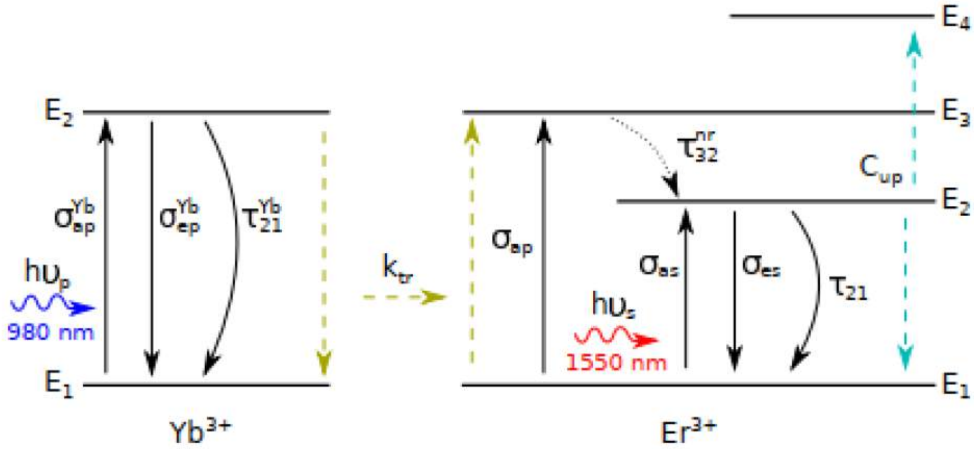

Figure 2.15 - Er^{3+} and Yb^{3+} Simplified energetic levels and transitions [18]

In the figure 2.15 the main characteristics of the ions, on which the different optical phenomena depend, are also reported: the cross section of absorption (σa) related to the photon absorption phenomena, the emission cross section (σ_e) related to photon emission phenomena, the lifetime (τ_{21}) relative life time of the excited states, the energy transfer coefficients (ktr), and up-conversion coefficients (Cup).
This model highlights efficiently the system generated by the co-doping of ions Er^{3+}, Yb^{3+}, that exploits thanks the peak in the absorption cross section (σaYb), a pump wavelength at 980nm. The absorbed energy is then transfered in a non-radiative manner to an adjacent Er^{3+} ion, to be consequently subject at first to a strictly not-radiative process (τ_{32}^{nr}) from level 3 to level 2, and then to a highly radiative process from level 2 to level 1, that emits a light signal at a higher wavelength, equal to about 1550nm (this is always possible thanks the Er emission peak at 1535nm). All the radiative processes, included the last one of this model, are strictly influenced by the quenching phenomena, more precisely, all that undesired effects, that consist in a reduction of a particular electrons population at an excited state. It competes with the stimulated emission (breaking it). The mechanism consists in an interactions between two ions, that pass each other an electron, that decades from an ion excited state (donor), transferring energy to the second ion (acceptor) in a not-radiative way. The closer the ions are, the stronger this mechanism is. This phenomenon occurs macroscopically decreasing considerably the life time of the donor excited energy levels (huge excited state electron population reduction). [19]

Optical fibers

In this chapter the main properties of fiber optics will be reviewed. The first sections present in general their structure and main characteristics, whereas the last sections expose the fabrication techniques, and some special type of fibers in the perspective of the CALIBER project.

3.1 Overview

An optical fiber is a spatially inhomogeneous structure, that restricts the spatial region in which light can propagate. Since electromagnetic energy, once generated in one place, has a natural tendency to spread in the whole space at a speed close to 300.000 km/s (indicated by c), the optical fiber permits then a confinement of the light, for guiding it on a well-defined path.

3.1.1 Refractive index and total internal reflection

An electromagnetic wave that travels in a dielectric medium polarizes, through the oscillations of the electric field, the molecules of the material at the frequency of the wave. Consequently, the speed of light in a material is lower than that of the vacuum, where there are no dipoles with which the field can interact. The ratio between the light speed in the vacuum (c) and the light speed in a material (v) is the refractive index (n) of the material: $n = c/v$.
An electromagnetic wave propagating in a medium, that approaches the separation interface with a second material, splits in a reflected component that propagates backward towards the first medium, and in a transmitted wave that propagates forward in the second medium (figure 3.1). The relationship, between the refractive indexes and the angles of incidence and refraction (the suffered deviation in crossing the separation surface), is described by the Snell's law (equation 3.1):

$$\frac{n_1}{n_2} = \frac{sin\theta_2}{sin\theta_1} \tag{3.1}$$

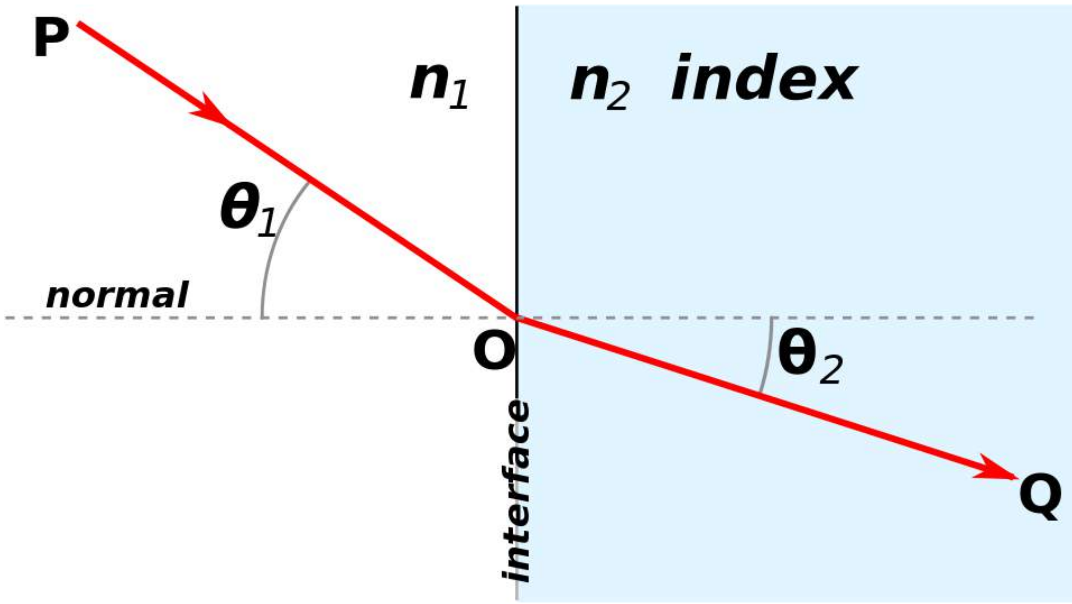

Figure 3.1 - Snell's law phenomenon, described by geometrical optics [21]

In the figure 3.1 θ_1 is the angle of incidence, and θ_2 is the angle of refraction. In general, if a light beam passes from a less dense material (low n) to a denser one (high n), it is bent towards the normal vector at the interface, and the angle of refraction will be smaller than the angle of incidence. In the opposite case, if a light beam passes from a denser material to a less dense one, it is bent towards the parallel vector at the interface, and the angle of refraction will be greater than the angle of incidence. Considering the last case, as the angle of incidence θ_1 increases, the angle of refraction θ_2 approaches the value of 90 degrees, until it reaches a point where refraction is no longer possible. Therefore, the ray of light is totally reflected back in the first material, and the light cannot cross the interface. This condition is called total internal reflection (TIR), and the angle at which it occurs is called the critical angle (equation 3.2) .

$$\theta_c = arcsin(\frac{n_2}{n_1}) \tag{3.2}$$

[22]

3.1.2 Optical fiber structure

In the simplest case, an optical fiber is a two homogeneous glass media structure. The media are called core and cladding. The core is the innermost part of the fiber, and is the area where the light is confined and propagates. The core is surrounded by a dielectric material (cladding) with a lower refractive index than the core. This condition is necessary to exploit TIR, to confine the light inside the fiber core. Moreover, since the optical fiber guides the light on one direction, the optical confinement is exploited on the other two directions.
Outside the cladding, there is typically a protective polymer coating, which improves the fiber

mechanical strength, and protects the innermost layers from humidity and environmental agents (figure 3.2). Such buffer coatings may consist of acrylate, silicone or polyimide, for example. At the fiber ends, the coating often has to be stripped off.

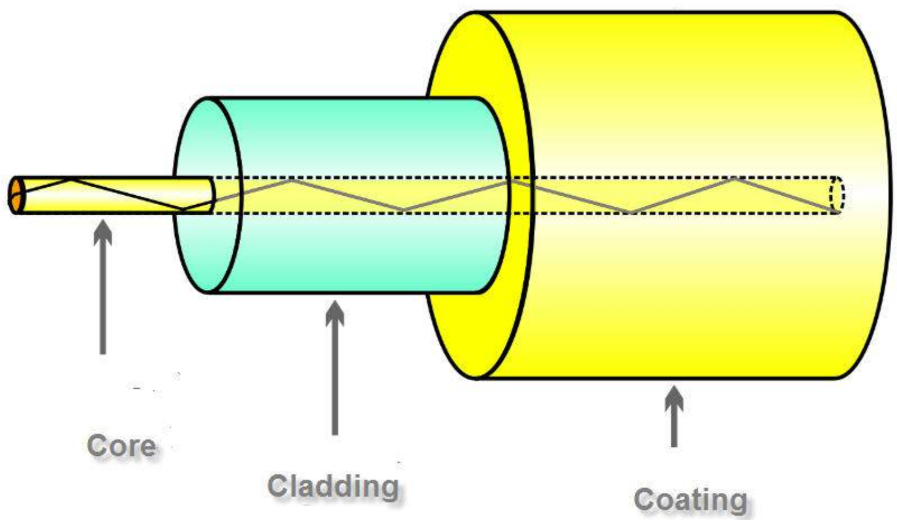

Figure 3.2 - Optical confinement inside the structure of a step-index fiber [23]

3.1.3 Fibers main parameters

An optical fiber can be described by several parameters, that indentify their characteristics.
One of these is the normalized frequency (V), an dimensionless parameter that describes the number of supported modes by an optical fiber. Propagation modes of a waveguide (an optical fiber generalization) are that field distributions, that maintain their transversal shape on the propagation direction. The modes linear combination describe in general the whole field. From the TIR condition, it can be demonstrated that it is obtainable a transcendental equation of dispersion, whose plot is depicted in figure 3.3.

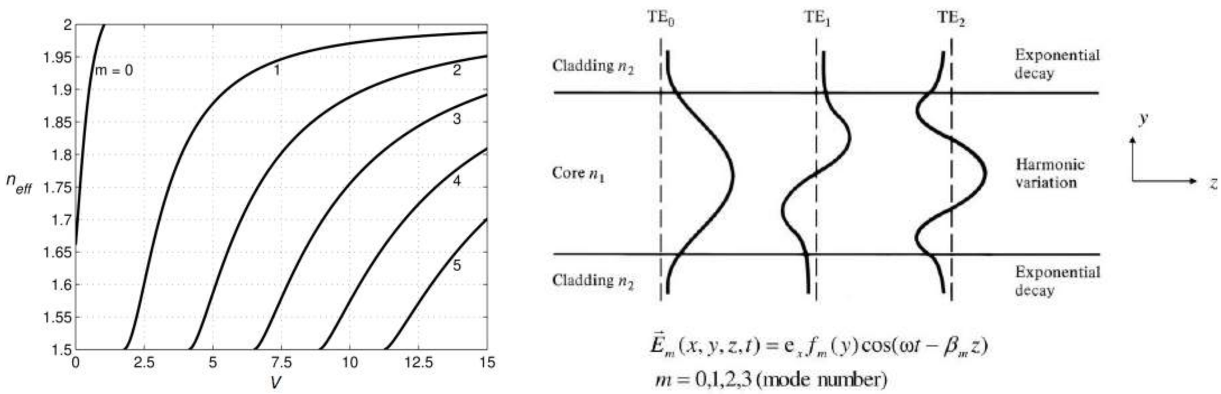

Figure 3.3 - Waveguide transcendental dispersion plot (on the left), and shape of first three modes (on the right) [24]

The plot 3.3 describes the relation between the optical and geometrical characteristics in a generic waveguide. Each curve is a different mode. The n_{eff} parameter is that particular refractive index, that a mode experiences propagating in the whole structure; if it is $n_{clad} < n_{eff} < n_{core}$ the mode is guided, otherwise it is radiated. As already mentioned, V (the normalized frequency) is that dimensionless parameter, that characterizes a waveguide structure. Consequently, the V knowledge permits to evaluate how many guided modes that structure is able to support. Indeed, it's demonstrable that for instance for a $V < 2.405$ the fiber is single mode (since only the first mode is supported), otherwise it's multimode.

An other important parameter is the numerical aperture (NA). The NA of an optical fiber is that dimensionless number, that characterizes the range of angles over which the optical fiber can accept light, in order to exploit TIR (figure 3.4). Mathematically, the index contrast between core and cladding determines the numerical aperture of the fiber (equation 3.3)

$$NA = \frac{\sqrt{n_{core}^2 - n_{cladding}^2}}{n_0} \tag{3.3}$$

n_0 is the refractive index of the medium around the fiber, and generally is air. The arc sine of the NA is called the acceptance angle, and is typically small, so that optical fibers are weakly guiding structures. [25]

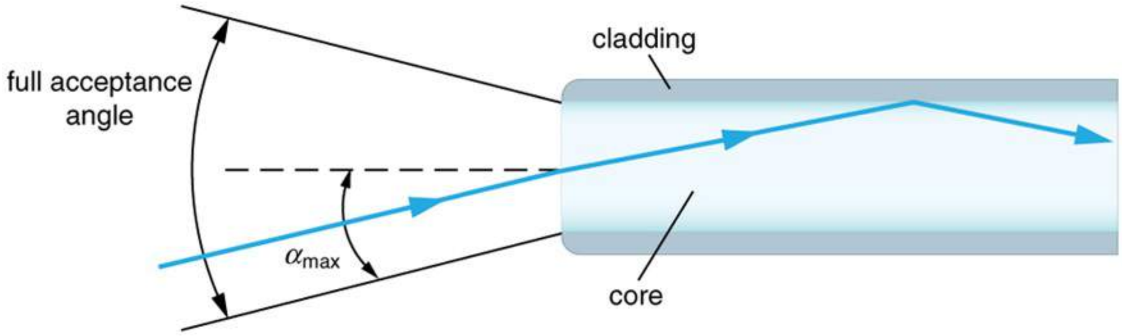

Figure 3.4 - Scheme of the acceptance angle of an optical fiber [26]

3.1.3.1 Attenuation

The attenuation is an optical phenomenon, defined as a power loss of a ray of light moving along a fiber. It is mainly caused by phenomena of absorption, scattering and bending losses. In an optical fiber of length L, an input power P_{in} and an output power P_{out}, the attenuation α is defined by the following equation 3.4.

$$\alpha_{dB} = \frac{10}{L} \cdot log(\frac{P_{in}}{P_{out}}) \tag{3.4}$$

The unit of measurement depends on the unit of measurement of the length, and can be expressed as dB/m or dB/km.
Absorption is one of the main causes of signal loss in an optical fiber. It is defined as reduction of optical power due to conversion into internal energy of the absorbent structure, for example in thermal energy.
An other cause of losses is the scattering, an unavoidable effect due to the interaction of light with composition fluctuations generated during the formation of glass. The light, passing through the fiber, interacts with these areas as if they are small particles of dielectric material, and is partially refracted in all directions. If the dimensions of these fluctuations are smaller than one tenth of the wavelength of light, Rayleigh scattering occurs. This type of scattering is inversely proportional to the fourth power of the wavelength of light, and is the main cause of losses in the area between UV and IR in silica fibers. If the dimensions of the fluctuations are compatible with the wavelength of light then, the Mie scattering phenomenon occurs, which is less dependent on the wavelength than the previous one.
Bending losses are classified, according to the curving radius of the bend, in micro and macro curvatures. The microbends are microscopic bending of the fiber axis, that often occur when the fiber is covered by the coating or improperly wired, causing small imperfections in the fiber. Microbends cause attenuation, because low order modes are coupled with high order modes, and can therefore exit the fiber. Otherwise, macrobend losses are observed when the fiber bending radius is large compared to the fiber diameter. This bending involves a change in the field of

modes, increasing the amount of field that cross the cladding, in this way part of the electromagnetic radiation is lost towards the outside. [25]

3.2 Fabrication methods

There are two main methods of fiber fabrication: double crucible drawing or preform drawing. The first produces a selected fiber by pulling the glass from two cavities, containing the core and cladding glasses in the molten state. This method is used for special glasses, where great purity is not required, and can only produce step-index fibers.

Most optical fibers are fabricated by pulling from a so-called preform in a fiber-drawing tower, an apparatus which is typically several meters high. The preform is a glass rod with a diameter of a few centimeters and roughly 1m length. Along its axis, the preform contains a region with increased refractive index, which will form the core. When the preform is heated close to the melting point in a furnace, a thin fiber with a diameter of typically 125μm and a length of many kilometers can be pulled from the bottom of the preform. During the pulling process, the fiber diameter is held constant by automatically adjusting the pulling speed and the furnace temperature, with an automatic feedback system, containing a diameter monitor.
Fiber pulling works quite well for the usual silica fibers, since silica has a rather broad glass transition: a large range of temperatures, where the viscosity is in a suitable range. Other materials, such as phosphate fibers, having a much smaller suitable temperature range for pulling, require more attention and care in the drawing process. [27]

3.2.1 Preform realization

Many fiber preforms, especially those controlled on silicate glass, are fabricated with a process called modified chemical vapor deposition (MCVD or just CVD), that basically consists in a modified version of the standard material deposition in vapor phase.
This method was developed for the telecommunications fibers in silica in the 70s. Thanks to the production from vapor phase, it is possible to obtain purity levels and very low propagation losses (<0.2dB/km). However, a major challenge in CVD production is required by the integration of rare earths in the preform, because of their reduced vapor phase volatility. [28]

In the case of preforms based on non-silicate glasses, whose precursors cannot be used in the vapor phase, the fabrication method typically used is the *rod-in-tube*. With this technique a rod (core precursor) of a glass with higher refractive index is inserted into a glass tube (cladding precursor) with lower refractive index (figure 3.5).

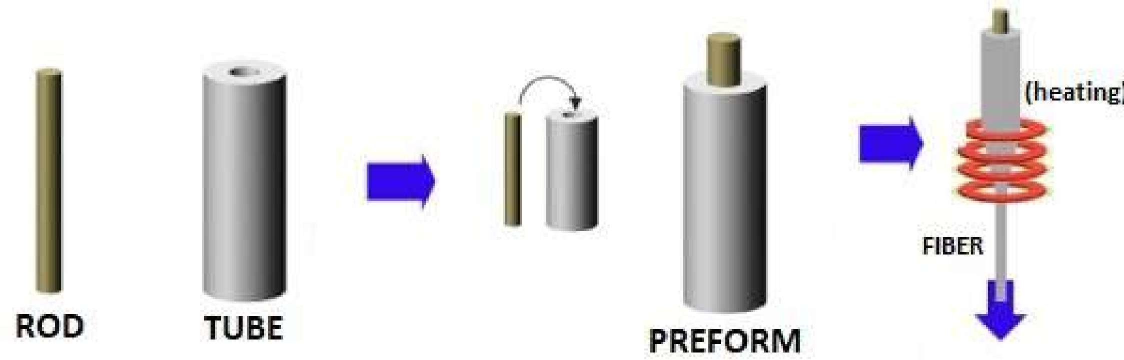

Figure 3.5 - Scheme of the rod-in-tube technique [29]

3.2.2 Drawing tower

Optical fibers are fabricated by the preform through a drawing process. This process allows the reduction of the preform diameter up to the size of the fiber, without changing the optical properties, and the refractive index profile realized into the preform.
In vertical drawing conditions, diameter reduction occurs at a temperature higher than the glass softening temperature. The choice of the drawing temperature is based on numerous factors, including for example the type of glass and dopants, the diameter of the fiber to be obtained, the drawing speed and the dimensions of the heating furnace.
By controlling the inserting speed V (μm/s) of the preform inside the furnace, and the drawing speed of the fiber v (m/min), knowing the diameter of the preform D, it is possible to calculate the estimated diameter d for the fiber, through the following equation: $D \cdot V = d \cdot v$. The area, where the diameter is reduced, is called neck-down, and corresponds to the area of the greatest temperature reached by the glass.

The dimensions of a drawing tower can vary from a few meters to more than 20m in height. The dimension variation is based on the characteristics of the fibers and the materials to draw. A drawing tower is typically composed of several parts, as shown in figure 3.6:

- A rigid vertical structure, which all the elements are secured to;
- A heating system for reaching high temperatures;
- A fiber diameter measurement system;
- An optional coating system;
- A drum to draw and collect the fiber.

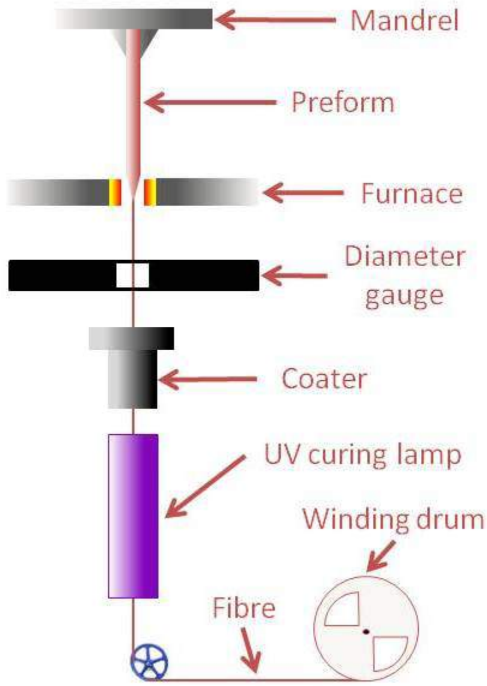

Figure 3.6 - General scheme of a drawing tower [30]

The drawing tower, used by the Photonext research team and located at LINKS Foundation, is the only example of glass drawing tower for research activity in Italy.

3.3 Optical fiber types

The wide variety of optical fibers allows different forms of classification, based on various criteria, such as the application, the material, etc.. However, one of the most widespread is based on the differences in the structure of the core and of the cladding.

3.3.1 Structural classification

The optical fibers can be classified on the base of the core size. Therefore, they are classified on the base of the supported guided modes: single mode fibers (SMFs), and multi mode fibers (MMFs).

SMFs have a relatively small core (with a diameter of only a few micrometers), and can guide only a single spatial mode, whose profile in most cases has roughly a Gaussian shape.
MMFs have a larger core, and/or a larger index difference between core and cladding, so that they support multiple modes with different intensity distributions (Figure 3.7).

Usually, long-range optical fiber communication systems use SMFs, because the different group velocities of different modes would distort the signal at high data rates. For shorter distances, however, MMFs are more convenient, because for their wider core size, the demands on light sources and component alignment are lower. Therefore, local area networks (LANs), except those for highest bandwidth, normally use MMFs. In general, MMFs are convenient for the transport of light from a laser source to the place where it is needed, in particular when the light source has a poor beam quality, and/or the high optical power requires a large mode area.

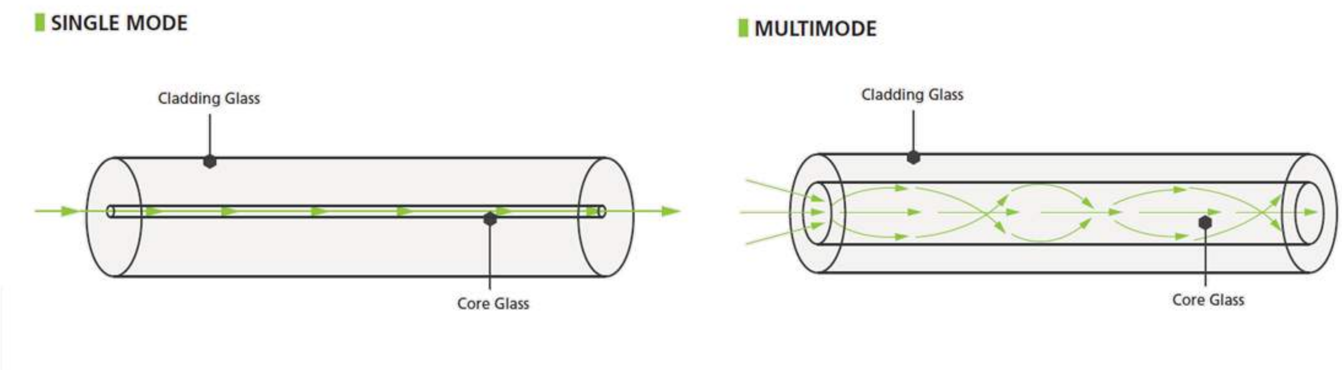

Figure 3.7 - SMFs and MMFs difference [31]

In addition to the core size, an other important structural parameter is the refractive index profile, that discriminates between step-index fibers and graded-index fibers.
Step-index optical fibers are the optical fibers simplest case, where the refractive index is constant within the core and within the cladding. The graded-index fibers have instead their core refractive index continuously changing radially from the center of the core to its surface.

Although most optical fibers have only a single core and a single cladding, there are also so-called multi-core fibers containing a few cores or even a large number of those. The whole set of these multi-glass fibers takes very often the name of microstructured optical fibers (MOFs). The MOFs term includes all those fibers, whose structure of the waveguide is used at a nano-scale level to manipulate light. Some examples can be: photonic bandgap fibers, where the light guiding is based on a photonic bandgap (a structure with a periodic core refractive index profile) or double-cladding fibers (DCFs). [32]

DCF or air-cladding fiber is an optical fiber, with a structure consisting of three layers of dielectric material, instead of the usual two. The inner-most layer is the core, that is surrounded by an *inner cladding*, which is surrounded again by an *outer cladding*, (that is air for air-cladding fibers). The three layers are made of materials with different refractive indices. DCF is an important technology in the area of active fiber optics, particularly for high-power fiber lasers and amplifiers.

Inside a fiber amplifier, the stimulated emission condition, that provides optical amplification, it's mantained with an active dopant pumping with power from a pump laser, whose light in general propagates through the fiber core, together with the signal to be amplified (figure 3.8). Therefore, inside a DCF the pump light: is restricted to the inner cladding by the outer cladding (with lower refractive index), and also partly propagates in the core, where it can be absorbed by the laser-active ions. This pump injection type in the device is called *cladding pumping*.

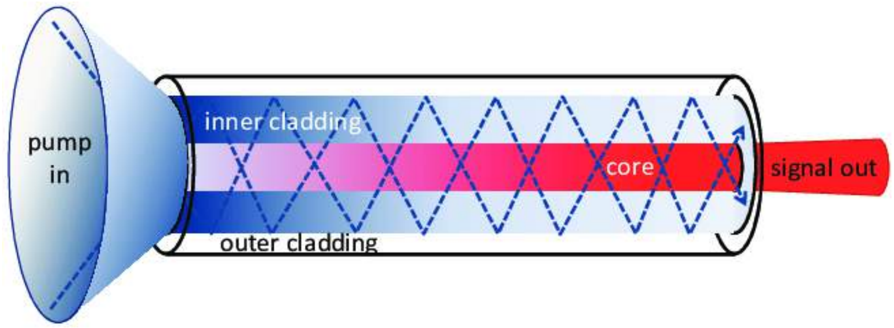

Figure 3.8 - DCF optical amplification principle [33]

3.3.1.1 CALIBER project fiber

In conclusion, summarizing the previous chapter concepts, the fiber, that was deemed more appropriate to satisfy the CALIBER project specifications, is:

- a phosphate one, because it provides the best performance in terms of optical amplification length, thanks their outstanding solubility of laser active ions.
- a multi-mode one, because the alignment with the source is easier and the pump power density is lower.
- an air-cladding one, because its structure presents high performances in the area of power amplifiers.

Amplifier realization and characterization methods

This chapter reports on the adopted approach to realize and test an optical amplification bench, whose power amplifier is an ytterbium-erbium doped fiber (YEDF). This chapter is structured in two sections: while the first briefly presents the YEDF realization and characterization, the second exposes the main steps carried out to develop the optical amplification bench, with the integrated YEDF.

4.1 YEDF realization and characterization

The first step to realize an EDFA is the design of a robust and stable host glass, which is able to support high amounts of rare earth active ions and a drawing tower process.
As it was explained in section 2.3.2, the Yb rare earth ions, working as acceptors, absorb pump laser energy, and transfer it to the Er, in order to provide stimulated emission condition. Consequently, it arises that the greatest optical amplification results occur for high Yb ions concentrations.
Therefore, the host glass choice was relapsed to a phosphate one for compactness reasons. This choice enables the realization of an active medium with high optical gain in short length (> 5 dB/cm), mitigating nonlinear optical effects. Moreover, this glass type possesses a large glass formation region, and good thermo-mechanical and chemical properties.

4.1.1 Rod fabrication

The fabrication, conducted in the Glasses for Photonics Lab (located within the DISAT), started from extremely pure and hygroscopic powders. The reagents considered were: P_2O_5, K_2CO_3, Al_2O_3, La_2O_3, B_2O_3, $BaCO_3$, PbO, Gd_2O_3, Er_2O_3 and Yb_2O_3, where:

- P_2O_5 is the oxide forming the glass structure,

- Gd_2O_3, Er_2O_3 and Yb_2O_3 are the rare earth ion precursors,
- and the other reagents are modifier elements, properly inserted into the glass composition to obtain required thermodynamic, optical and mechanical properties.

The concentrations of Er and Yb ranged respectively between 1%-3%, and 2%-8%. Therefore, the ratio between erbium and ytterbium ions concentrations ranged between 1:2 and 1:8. The glasses were produced through a *melt quenching* technique.

4.1.1.1 Melt quenching

Melt quenching was the first glass preparation technique, used in glass industry as well as in research field, before chemical vapor deposition (CVD) and sol gel technique. One of the important features of the melt quenching method is the flexibility of preparing a large number of glass compositions of silicate, borate, phosphate, oxide or non oxide systems. Using this method, the doping or co-doping of different types of active ions is relatively easy. Compared to other glass preparation methods, the disadvantage is the lack of purity of the prepared glass sample. In order to avoid contaminations, crucibles made of noble metals like Gold, Platinum etc are used. [34]
Typically, the melt-quenching technique includes: mixing of ingredients, heating up to a temperature usually higher than 1300 C, and quenching of the melt glass to obtain a glass bar. So basically, the melt quenching technique is a molten glass casting process in a cylindrical mold (figure 4.1).

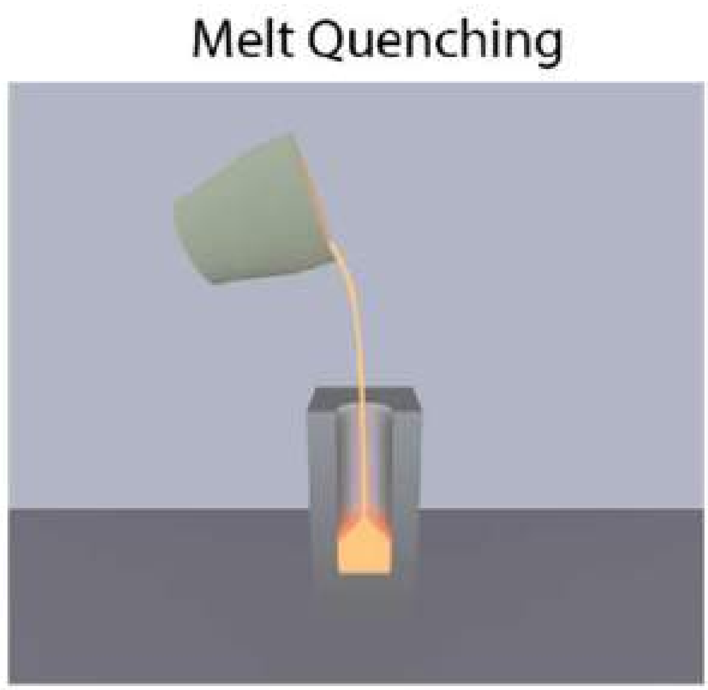

Figure 4.1 - Simple scheme of molten glass casting process in a cylindrical mold

For the fabrication of the CALIBER glasses, the reagent powders were placed into an alumina crucibles, and were inserted in a furnace to reach the melting temperature (1400 C for 1h). The melt glass was casted on a metallic plate and, thanks to a fast cooling, it suffered a thermal shock. Consequently, the cracked glass was placed into several crucibles, and was melted a second time. Finally, the glass was casted on a cylindrical brass bar, pre-heated at 400 C. The glass inside the mold was, one more time, annealed to relieve internal stress.
The powders extremely hygroscopic characteristic may strongly compromise optical properties, because the water OH^- molecules act as quenching centers of the excited states (section 2.3.2). For this reason, during the whole process, it was dedicated particular attention to possible contaminations from water or atmospheric humidity.
Three different doped glass compositions were designed and realized, with a fixed level of Er_2O_3 (0.75 mol%) and an increasing level of Yb_2O_3, ranging from 1.50 to 4.50 mol%,. Therefore, as summarized in the table 4.1, the Er-Yb concentration ratio was 1:2, 1:4, and 1:6.

Glass name	$Er^{3+}[10^{20} ions/cm^3]$	$Yb^{3+}[10^{20} ions/cm^3]$
YE_1 **(1:2)**	**1.93**	**3.86**
YE_2 **(1:4)**	**1.92**	**7.69**
YE_3 **(1:6)**	**1.92**	**11.50**

Table 4.1 - Er-Yb glasses doping concentrations

The EDF composition, integrated in the set-up, was realized from the 1:2 composition. Once realized, the cylindrical rods were then cut by a diamond coated disc blade, located within the glasses laboratory, to obtain 2mm samples with parallel faces. Subsequently, the fabricated glasses were optically polished to 1mm-thick samples

Since the optical fiber is fabricated by drawing a preform, obtained by the rod-in-tube technique (section 3.2.1), it was, consequently, necessary fabricating a glass to realize the optical fiber cladding.

4.1.2 Tube fabrication

The fabrication of the tube requires an appropriate attention, because:

- The geometric relationships between core and cladding of the preform are identical to the ratios obtained in the final fiber.
- To allow a correct drawing process the cladding glass must have the same thermodynamic properties of the core glass. In particular, in order to obtain an homogeneous glass flow during the drawing, it is necessary that both glasses reach the same viscosity value at the same temperature. Moreover, during the cooling of the fiber from the drawing temperature, the two core and cladding glasses must be deformed in a similar manner as the

temperature changes. The coefficients of thermal expansion must, therefore, be very similar.

- To preserve a correct performance of the optical properties of the fiber, the cladding glass refractive index must be less than the core glass (section 3.1.1).

Currently, the cladding glasses, produced at the DISAT laboratory, are fabricated through a process of rotational casting. This manufacturing method allows the production of hollow tube-shaped preforms, with good dimensional accuracy, starting from the molten glass.

4.1.2.1 Rotational Casting

Rotational casting is a cost-effective casting technique, that is typically used for manufacturing of cylindrical and tubular parts. The method is used in the casting of metals such as steel alloys, magnesium alloys, etc., and non-metals such as ceramics, plastics, glass.
In the glass fabrication perspective, the centrifugal force, induced by the rotation, pushes the molten glass against the mold wall, where it solidifies (figure 4.2). This technique is time-saving, because it does not need guiding elements to direct the glass flow. Moreover, it produces quality castings in terms of accurate dimensions, good surface finish and porosity, because gas porosity is limited in the region of the cast surface. [35]
There are two types of rotational casting processes: vertical type and horizontal type. If rotational axis is vertical then it is vertical casting, and if rotational axis is horizontal then it is horizontal casting. Vertical rotational casting machines are used for gear blanks, pulley sheaves, brackets, wheels, and other mechanical components. Vertical casting can also be used to manufacture parts, that are non-symmetric, as well as non-cylindrical.
Horizontal rotational casting machines (as the one located, within the Glasses for Photonics Lab) are generally used to make simple geometries like cylinder bushing, pipes and tubes. [36]

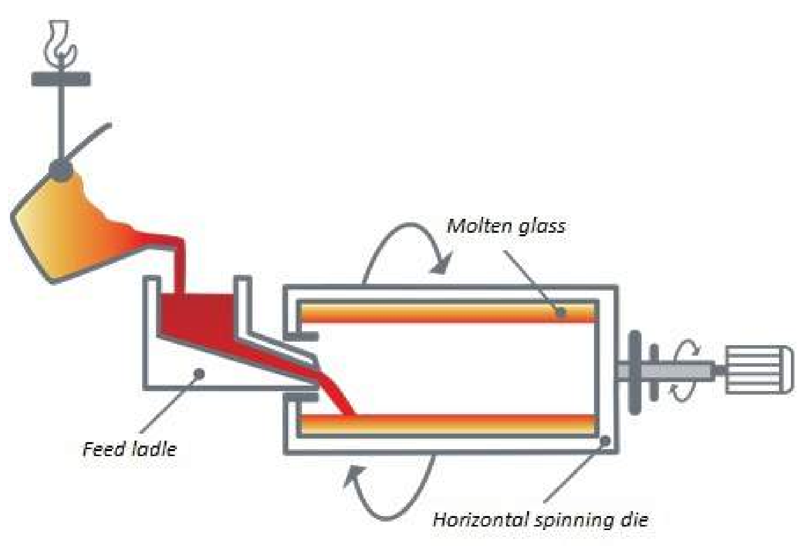

Figure 4.2 - Horizontal rotational casting working principle [37]

In the glasses fabrication, rotational casting is a technique, where reaching an effective uniformity of the final casted glass is strongly related on the flow pattern of the molten glass. Usually, true uniform cylinders are possible to generate more easily, at low rotational speed. Moreover, setting properly the rotation velocity of the mold, on the base of the glass mechanical properties, it's also possible controlling the glass cooling rate.

Once the tube was realized, the core and cladding glasses were cleaned and polished, in order to obtain an optimal contact in the preform assembly. Therefore, the realized preform was drawed into an optical fiber in a special drawing tower.

4.1.3 Optical fiber fabrication

A drawing tower is composed of two main parts: an area, where the preform is heated up to a temperature higher than the softening temperature, and a rotating drum, that allows to pull the obtained fiber, according to a controlled speed. The ratio, between the velocity of inserting the preform into the heated area and the fiber pulling speed, defines the reduction ratio of the fiber section (section 3.2.2).

Once the softening temperature is reached, the glass gains a viscosity such as to deform due to its own weight. Due to this deformation, a narrowing zone is created in the preform, called neck. The massive part of the preform, downstream from the narrowing area, applies a tension to the molten glass, due to its own weight. This downward traction decreases more and more the size of the neck area, that becomes a fiber. The fiber is then clamped onto a rotating drum, which imposes a calculated traction speed to obtain a given section size of the fiber. Therefore, the rotating drum imposes the drawing speed while collecting the fiber on itself. [38]

Here in figure 4.3, an image of the drawing tower is depicted.

Figure 4.3 - The drawing tower of the Photonext labs

During the process, it was necessary to control the tension, that was applied to the fiber during the drawing. Moreover, the diameter of the fabricated fiber, was monitored, through an optical diameter meter.

With a targeted Numerical Aperture (NA) of 0.11 for the optical fiber, the glass composition YE_1 for the core and one of the developed glass compositions for the cladding were used. The optical fiber (YEDF) was fabricated in three different dimensions (core/cladding diameters): 50/125, 78/195, and 100/250μm. The 100/250μm multi-mode one, thanks its size, was considered the most suitable for the CALIBER project. For this reason, it was at first characterized, and consequently integrated in the optical amplification set-up.

4.1.4 YEDF characterization

After having inspected, quality and morphology of the fabricated YEDF by means of an optical microscope, a set of near-field images of the fiber cross-section was measured on a 120 cm-long fiber piece, at the wavelength of 1300 nm, using an end-face coupled fiber pigtailed laser diode source, in order to assess the guiding properties of the fiber. Moreover, the fiber losses were measured by a *cut-back* technique.

4.1.4.1 Cut-back technique

The cut-back technique is a measuring method of the total attenuation of an optical fiber.
The attenuation of an optical fiber is the loss of optical power as a result of absorption, scattering, bending, and other loss mechanisms as the light travels through the fiber (subsection 3.1.3.1).
The cutback method involves comparing the optical power, transmitted through a longer piece of fiber, to the power, transmitted through a shorter piece of the fiber.
The cutback method requires that a test fiber of known length (L_y) be cut back to a shorter length. It needs access to both ends of the fiber. The cutback method begins by measuring the output power P_y of the test fiber of known length L_y. Without disturbing the input conditions, whose power is well known, the test fiber is cut back to a shorter length (L_x). The output power P_x of the short test fiber is then measured, and the attenuation coefficient (α) is calculated, through the attenuation formula 4.1.

$$\alpha_{dB} = \frac{10}{L} \cdot log(\frac{P_x}{P_y}) \tag{4.1}$$

Where $L = L_y - L_x$. [39]
Therefore, the fiber, wrapped as less as possible (to avoid bending losses), was periodically 5cm handy-cut, in order to estimate the attenuation α, through a weighted average of measurements of P_x and P_y for different lengths L.

4.2 Optical bench development

Once assessed the YEDF guiding properties, it was possible starting the development of the optical amplification bench. The set-up, that was deemed more appropriate accordingly with the laboratory available instrumentation, was designed as showed in figure 4.4.

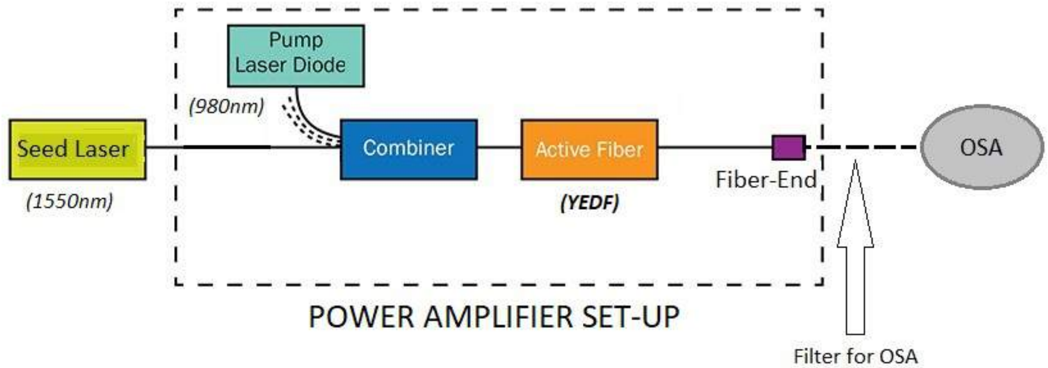

Figure 4.4 - Optical amplification bench designed

The employed seed was a continuous wave (CW) single-mode laser diode (center wavelength of 1542.5nm) with an input of 1mW. This seed was connected with a multi-mode pump laser (center wavelength of 976nm), by means of a pump combiner, that, basically, is a passive device where the power from several output fibers (such as the pump and the seed) is connected, and then distributed among a smaller number of input fibers, (one for this application).
The output of the pump combiner was butt-coupled to the YEDF with a 3-axis precision stage, that is an opto-mechanical component that exploits an effective fibers alignment, through a micro-movements system. Finally, the YEDF ouput was analyzed through an OSA, whose input port was protected, by the pump high powers, through an high pass optical filter.

4.2.1 Cleaving and splicing

The main procedures of an optical laboratory, necessary to develop any fibers-connected system, often rely to the cleaving and splicing operations of the optical fibers.

4.2.1.1 Cleaving

A fiber, made of active glass material, in order to amplify the optical signal, needs to be integrated into a system capable of conveying the pump and signal light inside it, with the smallest loss possible. A system, particularly robust and efficient, is the one made in an all-fibers configuration, that is, consists entirely of optical fibers. In this type of system the active fiber must be coupled with the other fibers through a junction process, paying attention to aligning the cores.

It is necessary that both sides of the fibers considered have excellent geometric and surface quality.
To achieve an optimal interface, a cleaving process is carried out, that is, the deliberate and controlled break of an optical fiber, in order to create an effective perpendicular interface to the fiber axis.
In general, cleaving process involves a technique called scribe-and-tension. The fiber is initially incised on its surface creating an initial crack (scribe), then a tension load is applied near the crack (tension). Therefore, the tension leads to a break of the fiber (figure 4.5).

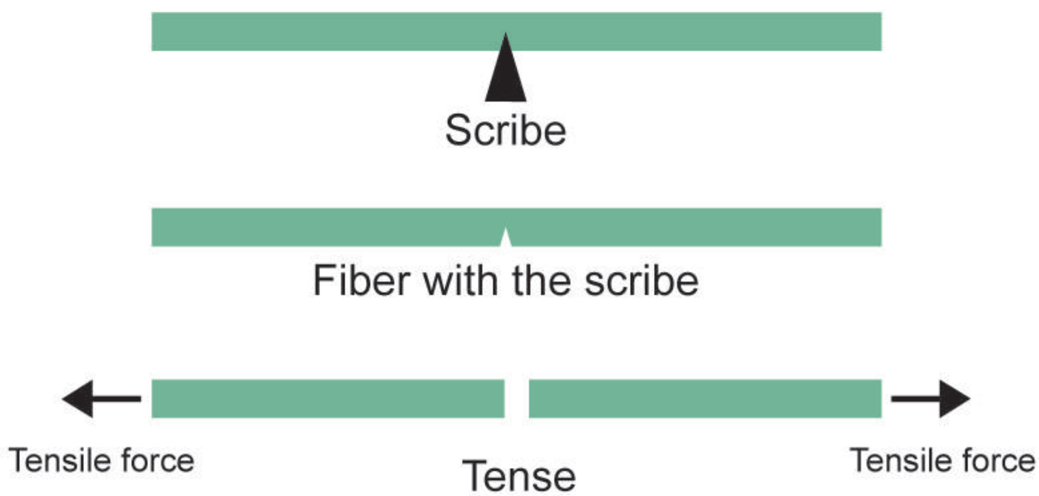

Figure 4.5 - Scribe and tension technique [40]

A generic scribe-and-tension cleaving process is represented in figure 4.5. The surface crack is usually created by inciding the fiber by a high-hard material, such as a diamond blade, sapphire or tungsten carb. Fiber breaks, on the other hand, can occur in different ways depending on the tool used. The laboratory instrument, that allows the cleaving of optical fibers, is called cleaver. More compact and manual instruments break the fiber, thanks to a bending of the fiber near the crack. More complex and automated cleavers allow to break the fiber, by applying a load of longitudinal traction, in order to increase the size of the surface crack.

In this research work, the tool used as cleaver was the 'Large Diameter Optical Fiber Cleaver CT-106' by Fujikura in the Photonext laboratory (figure 4.6). The instrument, blocking the fiber between two clamps, works automatically applying a tension on the fiber. Consequently, the crack is realized through a cutting blade, that incides transversely. The combination of blade advancement in the material, and the application of a tension on the fiber, allows to obtain a break with optimal surface and geometric qualities.

Figure 4.6 - Optical Fiber Cleaver of the Photonext labs, within the LINKS Foundation (on the left). A picture of a phosphate glass fiber during the cleaving process (on the right)

The instrument was equipped with a series of recipes for commercial silica glass-based optical fibers. There were created recipes for the controlled break of phosphate-based fibers, that have lower mechanical properties than silica-based fibers.

4.2.1.2 Splicing

The fusion splicing process consists in the end to end union of two fibers, through a glass fusion process. The goal is to weld two fibers together, so that light can pass from one to the other with limited loss phenomena. Schematically, the process proposes to put in contact the two final surfaces of the fibers to be welded, and heat the glass while applying a transversal pressure, in order to join the two fibers. The heat source used can be a laser, but usually is an electric arc.

A classic splicing cycle includes a series of coordinated steps, that are related to the power injection by the electric arc, and to the movement of the fiber-holders, where the two fibers are positioned. Once the fibers are locked in the fiber holders, and the instrument settings are selected, the two fibers are faced, and maintained at a certain distance. The default position is symmetrical, compared to the point, where the arc injects power. Therefore, the fibers are positioned at the electrodes. A first cleaning arc with reduced power is discharged onto the fiber in a short time, to eliminate possible dust particles present on the surface of the fibers. To maintain the ability to guide light through the interface, the two fibers must be aligned according to the core.

The splicing instrument can be set to align automatically the fibers, according to the position of the core or the cladding. Once the alignment is done, the fibers are positioned in contact. By changing the gap and overlap values of the instrument, it is possible to check the distance and intensity of the contact between the two faces.

A pre-fuse arc is applied for a short time, in order to initially decrease the viscosity of the fiber, and improve the contact between the surfaces. Consequently, the main fusion arc, characterized by a greater power and a considerably longer application time, is applied. Thanks to the main arc, in fact, the two fibers reach a temperature close to the softening temperature, and the glasses can be melted together. Subsequent to the fusion process, it is possible to carry out secondary remelting processes (re-arc), or continue with tapering processes in order to decrease the fiber size in a controlled manner. Therefore, the combined fiber can be taken from the instrument and tested.

In this research work, the adopted splicer was the: 'Fujikura FSM-100P Splicer' (FSM-100P) of the Photonext laboratory (figure 4.7). The figure 4.7, in addition to the FSM-100P splicer, depicts an other Fujikura fusion splicer (FSM 40-S). Compared to the FSM-100P splicer, that allows more flexibility in the recipes modes, and more efficiency for different glasses types (not silica-based), the FSM-40S one is less suitable, and fits only for commercial silica-based fibers. However, thanks to its portability, the FSM 40-S splicer was highly employed on the optical physical bench, to display and investigate the quality of the fibers interfaces.

Figure 4.7 - Fujikura FSM-100P (on the left). A picture of two prepared fibers at the end of a splicing process, with a FSM 40-S splicer (on the right)

4.2.2 Set-up realization

The work started from a 976nm LIMO pump laser, that was mounted over a cooled breadboard, controlled by a standard laser controller. Its P-I curve was investigated by two power meters: a Thorlabs one sensitive to low powers (up to 1W), and a Coherent FieldMaster one, which is able to support higher powers. The output fiber was mounted on a 3-axis precision stage, whose micro-movements control has allowed to maximize the alignment, thus minimizing the losses with the fiber input of the pump combiner, that was, subsequently, inserted.
The combiner fiber input dedicated to the signal, with a 8/125μm core/cladding diameters, was cleaved and spliced with a commercial pigtail single mode fiber, with 5/125μm core/cladding diameters size. Therefore, the commercial connector was inserted into the CW seed laser input port.
The signal input, the pump input and the output fibers of the combiner were precisely cleaved through the Fujikura cleaver, in order to allow an effective splicing operation. Moreover, a correct cleaving allows an alignment with 3-axis precision stage, without undesired reflections due to angled or rough interfaces. The output combiner fiber is a multi-mode one, with 105-125μm core-cladding diameters. Considering its diameter sizes, the choice to adopt the 100μm core size YEDF, among the fabricated fibers, was confirmed to be the most effective in the perspective of reducing coupling losses.
Consequently, the fabricated YEDF was cleaved, with particular recipe for phosphate glasses. The YEDF was realized as short as possible (4.5cm), to stick completely on the holder of 3-axis precision stage. The holder metallic surface allows a YEDF fast cooling process, avoiding thermical issues due to the usage of high pump powers. Therefore, the combiner output fiber was butt-coupled with the YEDF. Consequently, the power analysis at the YEDF end was performed through an OSA instrument. The OSA input port was protected by the 976nm high pump powers, through a Thorlabs high pass optical filter, with a 1000nm cutoff frequency (w_t), that was positioned immediately after the YEDF. Here in figure 4.8, a picture of the whole developed system is depicted.

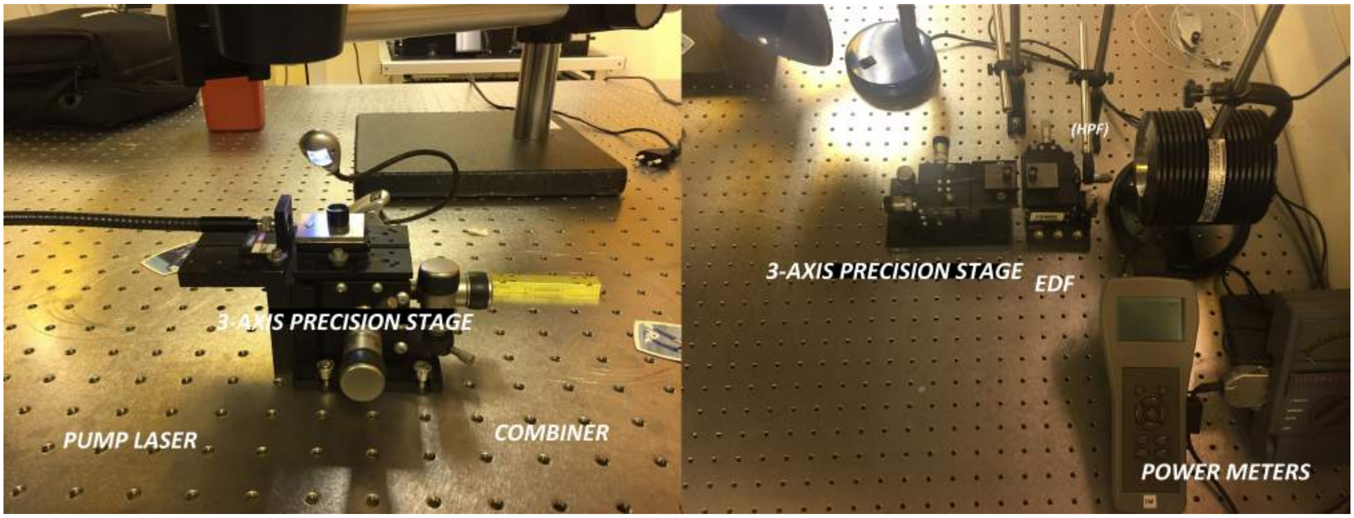

Figure 4.8 - Picture of the whole developed system

All the power measurements were performed after having adopted proper security measures, such as glasses and protection black screens, to avoid eye damages by laser reflections (especially by the pump one). In addition to the seed laser, the set-up was investigated by using an other low power laser source, emitting at 1300nm. The 1300nm laser source was adopted only to estimate the micro-positioning stage alignment losses, since at 1300nm the YEDF is transparent, and no power absorption phenomena occur at this wavelength. Therefore, the losses manifest themselves mainly for set-up misalignment reasons. About this, in order to reduce misalignment losses, that verify their selves exploiting 3-axis precision stages, the realization of splicing recipes to weld together phosphate glass-based fibers and silica glass-based fibers was carried on, thus to avoid lossy and time-spending inefficient air alignments.

Results

This chapter contains all the experimental results, obtained during the performed research activity.

5.1 YEDF characterization

The glasses fabrication, by melt quenching technique, produced three differently doped rods. In the figure 5.1 the rods are compared with the size of a pen. The three bars color is the same despite the different rare earths doping concentration. This peculiarity is explained by the fact that the only ion, that is responsible for the coloring of the glass is the Er^{3+} ion, which is in identical concentration in the three fabricated samples.

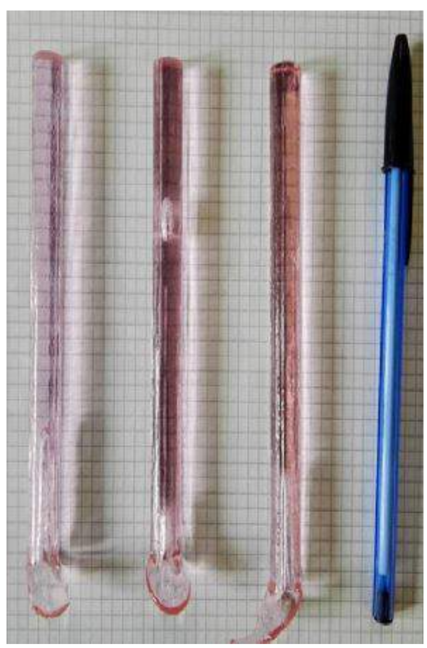

Figure 5.1 - A picture of the three fabricated cylindrical bars

The main physical and thermal properties of the fabricated glasses are exposed in the table 5.1.

Density	$3.43 \pm 0.05[g/cm^3]$
Glass transition temperature (T_g)	$502 \pm 3°C$
Crystallization temperature (T_x)	$762 \pm 3°C$
Glass stability parameter ($\Delta T = T_x - T_g$)	$260 \pm 6°C$
Coefficient of thermal expansion (α)	$0.000\,118\,7°C^{-1}$
Core refractive index at 1533 nm	1.565 ± 0.001

Table 5.1 - Physical and thermal properties of the fabricated glasses

Consequently, the estremities were cut with a disc blade, and the glasses were optical polished. Once the cladding was realized through rotational casting technique, the preform was realized using the glass rod with 1:2 Er-Yb compositions ratio.
Among the three dimensions of the fiber, drawn by the preform, the one with 100/250μm core/-cladding diameters size, was chosen for being used into the set-up.
The fiber was at first investigated through an optical microscope (figure 5.2).

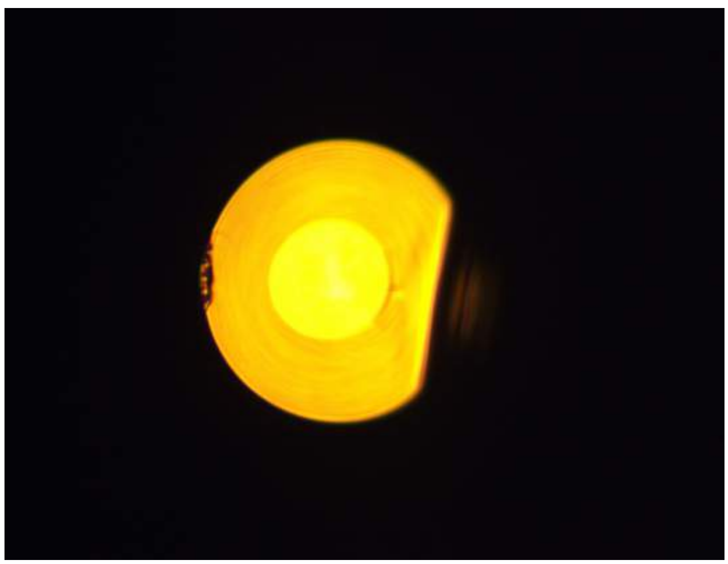

Figure 5.2 - An optical microscope picture of the 100/250μm multimode fiber

The figure 5.2 depicts the cross-section of the fabricated fiber (100/250μm). The absence of dark spots or bubbles, between core and cladding, has confirmed an efficient adhesion between the two different glasses.
A set of near field images were taken in order to evaluate the guiding properties of the fiber (figure 5.3). The light was found well confined in the core, thus confirming the good quality of the realized fiber. Subsequently, the fiber was investigated through a cut-back technique, in order to measure its attenuation losses.

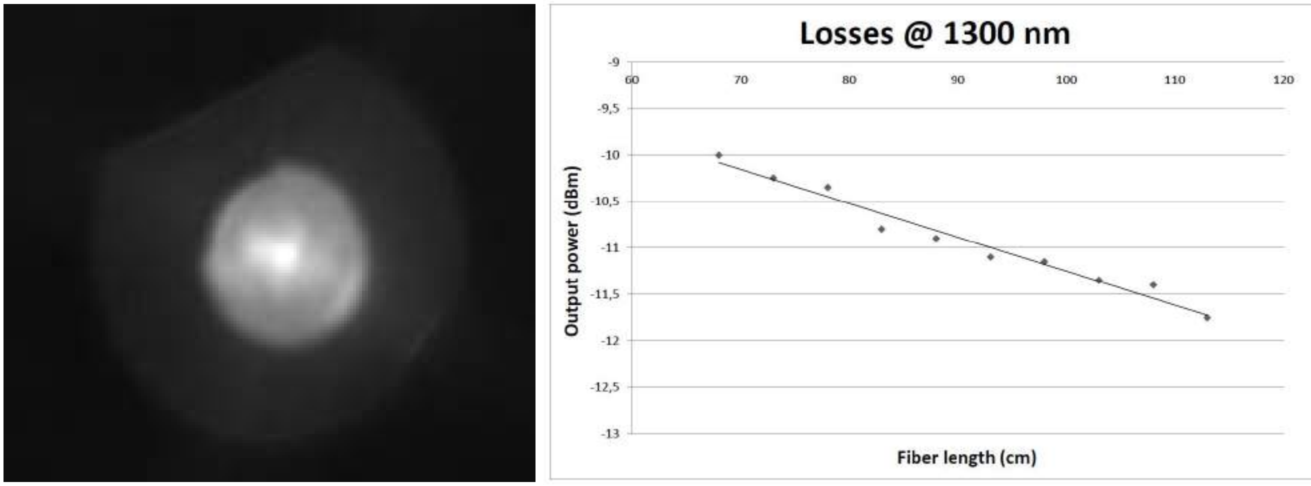

Figure 5.3 - A near field image (on the left), and its attenuation chart (on the right)

The attenuation value, as evaluated through a linear least square fitting of the experimental data, is $3.6dB/m$. This value is mainly due to absorption and scattering effects.
As expected, the result is considerably higher than silica attenuation losses ($0.2dB/km$); its application in telecommunications is unthinkable, but exploiting its peculiarities for centimeter distances on an optical amplification bench, this value is highly reasonable.

5.2 Set-up characterization

For the optical bench development, the first performed measurements were concerned the verification of the laboratory instrumentation. The table 5.2 and the graph (figure 5.4) compare the experimental results with the datasheet values. While the table 5.2 compares the individual low power laser values (1550nm and 1300nm), the chart 5.4 shows two curves for the current controlled high power pump laser (980nm). The match between the measured and the datasheet values has suggested a correct functioning of the instrumentation.

Laser source	**Datasheet**	**Measured**
1550nm	1mW	1.212mW
1300nm	0.5mW	0.512mW

Table 5.2 - Verification of the low power laser sources

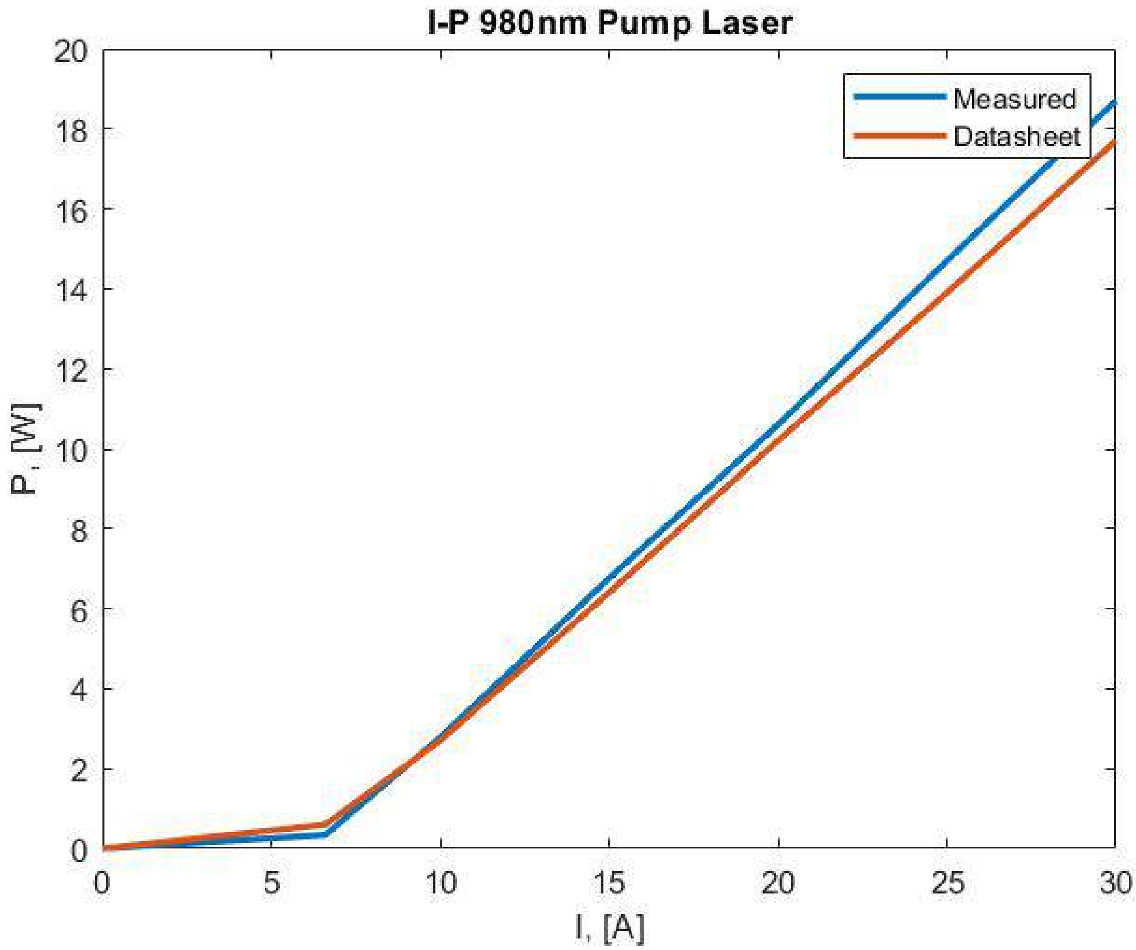

Figure 5.4 - Pump laser comparison between the experimental measurement and the datasheet curve

Once verified the lasers, the combiner device was inserted into the set-up. It was connected to the single mode fiber pigtailed seed laser source, through a splicing operation with 0.04dB losses. The pump was aligned with a 3 axis micro positioning stage. The combiner output power was investigated in order to know the precise amount of seed and pump power supplied at the YEDF, that accordingly to the scheme 4.4, is positioned next. Here in table 5.3 and in figure 5.5, the results of the low power lasers and of the pump are depicted, respectively.

Laser source	**Combiner input**	**Combiner output**	**Efficiency**
1550nm	1.212mW	0.837mW	**70%**
1300nm	0.512mW	0.453mW	**88%**

Table 5.3 - Combiner output power values with the low power sources

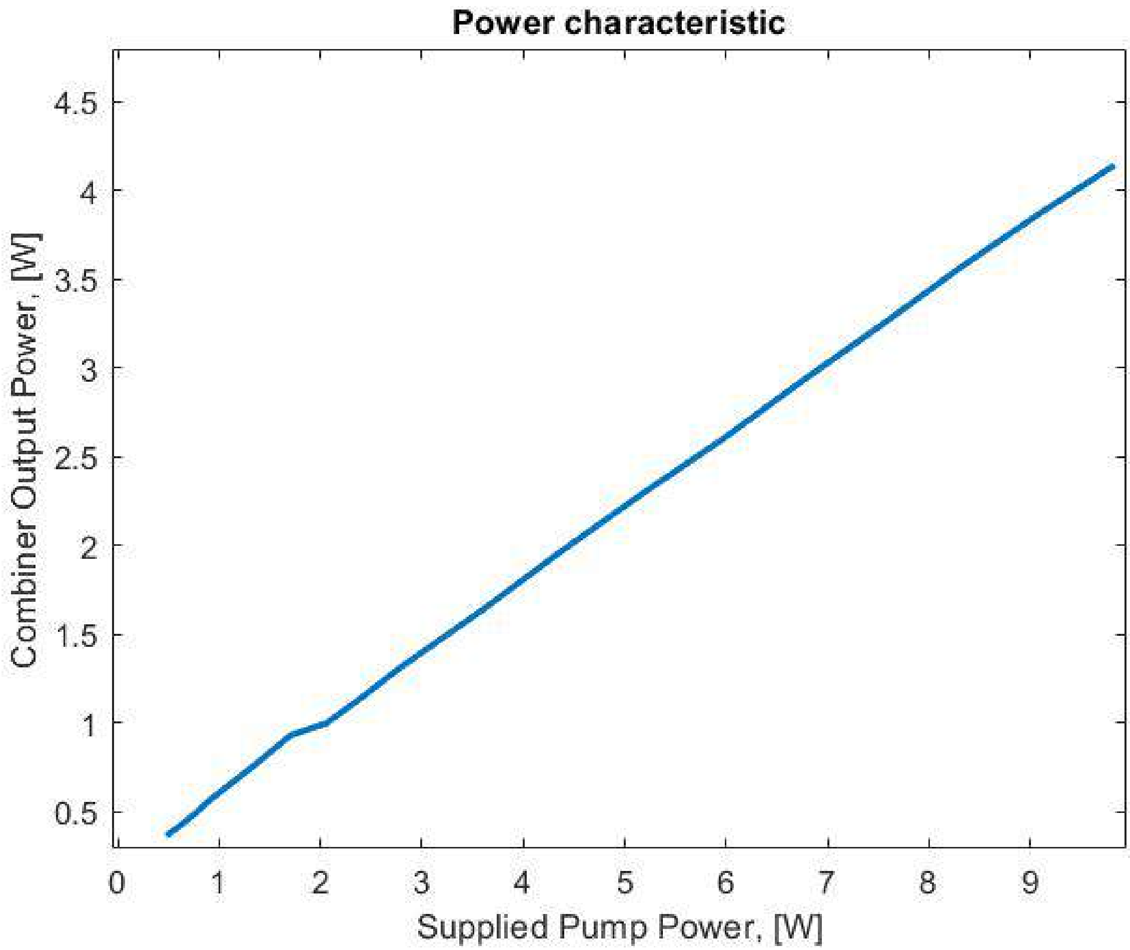

Figure 5.5 - Power Efficiency: Supplied Pump VS Combiner Output

As showed in 5.3, the table results present a propagation efficiency estimation. Considering that the combiner signal propagation efficiency is around of 93% (from datasheet), the 1300nm laser measurement is coherent with the expectation. However, the seed laser value that exploits a propagation efficiency of 70%, is lower than expected. Moreover, the pump graph in figure 5.5, highlighting a mean setup efficiency of 41%, defines certainly a non-performing alignment.

The estimation of the combiner output powers allowed the possibility to butt-couple the fabricated fiber, in order to evaluate, through an input and output powers analysis, the YEDF pump power absorption. The power measurements are exposed in table 5.4, and in figure 5.6.

Laser source	**YEDF input**	**YEDF output**
1550nm	0.837mW	0.589mW
1300nm	0.453mW	0.212mW

Table 5.4 - YEDF output power values with the low power sources

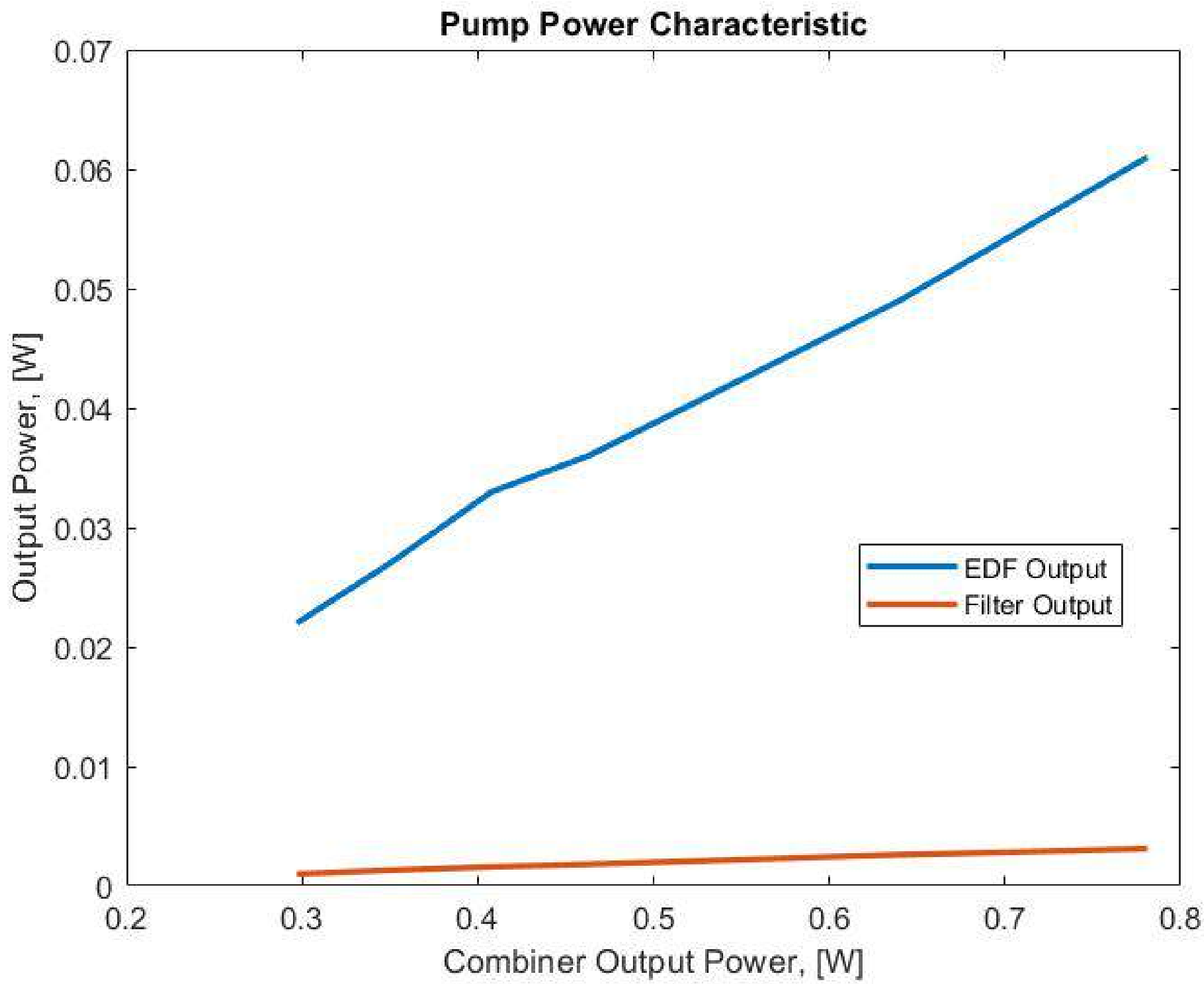

Figure 5.6 - Power Efficiency: Supplied Pump Vs YEDF Output

Since the YEDF is transparent at 1300nm wavelength, it is possible to assume that the attenuation of around 50% is mainly due to the coupling losses. Therefore, considering this 50% estimation, and that the pump figure 5.6 shows an output power attenuated by absorption and misalignment, it is obtainable, by excluding this last, a pump absorption efficiency equal to 80%. The high misalignment has considerably reduced even the low power signal value.

In the chart 5.6 it's also reported a second curve, depicting the pump signal after the high pass filter. The reasonably low obtained values do not represent a danger for the input port of the OSA, that has detected no remarkable amplification result, probably due to the high misalignment between the set-up elements, especially between the pump fiber and the associated pump combiner input. An approach, to improve the results avoiding the huge losses for air-alignment, could be to carry out extra splicing operations, even between phosphate and silica fibers, as it was made in the next section 5.3.

5.3 Cleaving and Splicing

The efficiency improvement of any fiber-connected set-up is possible, first of all, realizing acceptable cleaving and splicing operations.
In particular, effective cleaving and splicing, between a commercial-silica fiber and a phosphate one, can considerably boost the signal and pump propagation efficiency, because the misalignment losses, due to the fiber coupling through 3 axis micro positioning-stages, no longer occur.

5.3.1 Cleaving

The cleaving process is exploited through a transverse incision by a cutting blade, when the fiber is put in tension, blocked between two clamps. Therefore, in order to adapt the cleaving process for the phosphate fibers, it was indispensable to operate mainly on the clamps and blade parameters.
Here in figure 5.7, the characteristics of the implemented cleaving mode (recipe) are depicted.

Figure 5.7 - Cleaver recipe for CALIBER phosphate fibers

The recipe on figure 5.7 was designed to work on phosphate fibers with 100/250μm core/-cladding size. Each image represents a page, among the six programmable pages inside a cleaving mode.
In the first page, that shows the fundamental settings, the clamp diameters were set on the base of the phosphate fiber cladding diameter (250μm indeed). It is necessary, that these parameters match with the dimensions of the inserted fiber holders.
The second page, that regulates the clamp settings, was set with clamp forces equal to 3150gf.

This value is reasonably lower than the 4500gf one of the silica-fibers, that show higher mechanical properties than phosphate fibers. The choice of this number was taken after the execution of numerous tests, which have exposed that, low values of clamp forces caused fiber slips, and high values cracked the fiber.

Finally, in the third page the main modified parameter was the cleave tension. This parameter establishes the tension to reach, in order to start the incision with the cutting blade. It was set equal to 135gf, that again is considerably lower despite the 360gf one of silica-fibers. Low values of cleave tension can make the cutting blade incision ineffective, since the tensional load is too low. Otherwise, high values may imprecisely crack the fiber before the blade incision. The other cleaving mode pages, concerning the blade and angled cleave setting, were not modified.

Here in figure 5.8, an image of a correctly cleaved phosphate fiber is depicted.

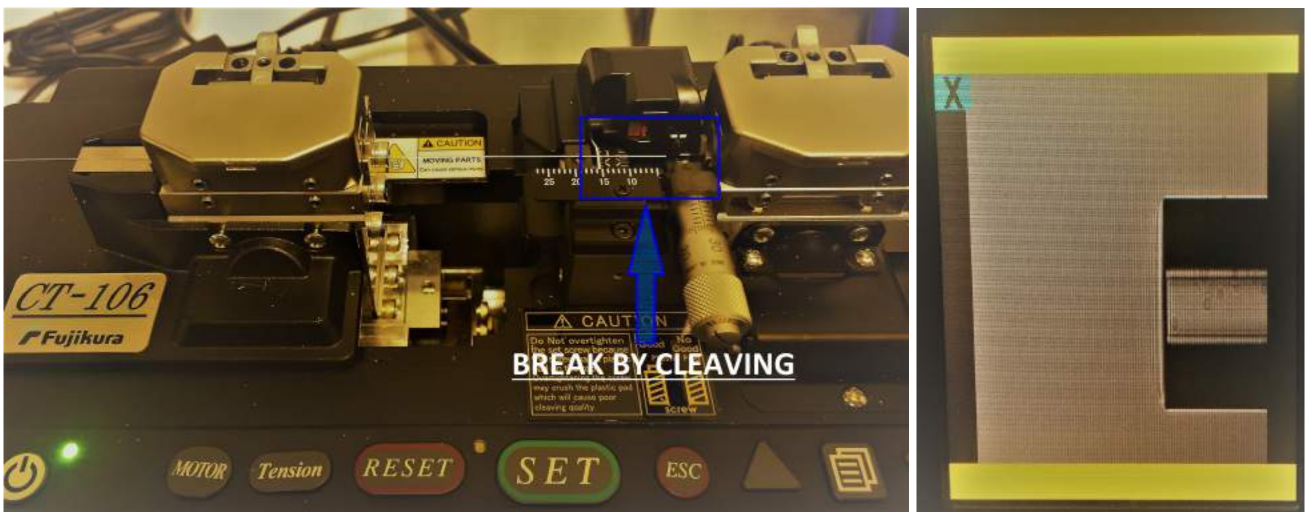

Figure 5.8 - Cleaved phosphate fiber (on the left), and its quality assessment through the splicer display (on the right)

5.3.2 Splicing

The splicing process is exploited positioning two fibers end to end, and injecting power by the electric arc. Therefore, in order to splice a silica-based fiber and a phosphate one, it was necessary to operate mainly on the arc, and on the fiber-holders motors parameters.
Here in figure 5.9, the characteristics of the implemented splicing modes are depicted.

Figure 5.9 - Splice mode for silica-fibers (on the left), splice mode for phosphate-fibers (on the right)

The left picture on figure 5.9 exposes the implemented splicing mode for two silica-based fibers. The recipe, for two 125μm cladding size fibers, essentially establishes: a XY motors movement based on a core alignment, and an arc power injection of 301bit for 2000ms. Moreover, the θ motors doesn't perform any alignment (so no rotation), and the distance between the electrodes is 1mm.
The right picture on figure 5.9 depicts, instead, the implemented recipe to splice a silica-based fiber and a phosphate-based one. While the silica fiber cladding diameter is 125μm (on the left), the phosphate fiber cladding diameter is 250μm (on the right). The second recipe alignment procedure, based on a claddings alignment, includes a rotation of the motors associated to the fiber holders, because the θ alignment parameter is not set to off, but to an angle offset ($Angle\ command$). The electrodes distance is maintained 1mm. Moreover, for the different thermic properties of the phosphate fiber, the arc power injection is performed for less time (1350ms), and at lower power (240bit) than previous recipe.
Here in figure 5.10, an image of a result of an efficient splicing operation with the second recipe is depicted.

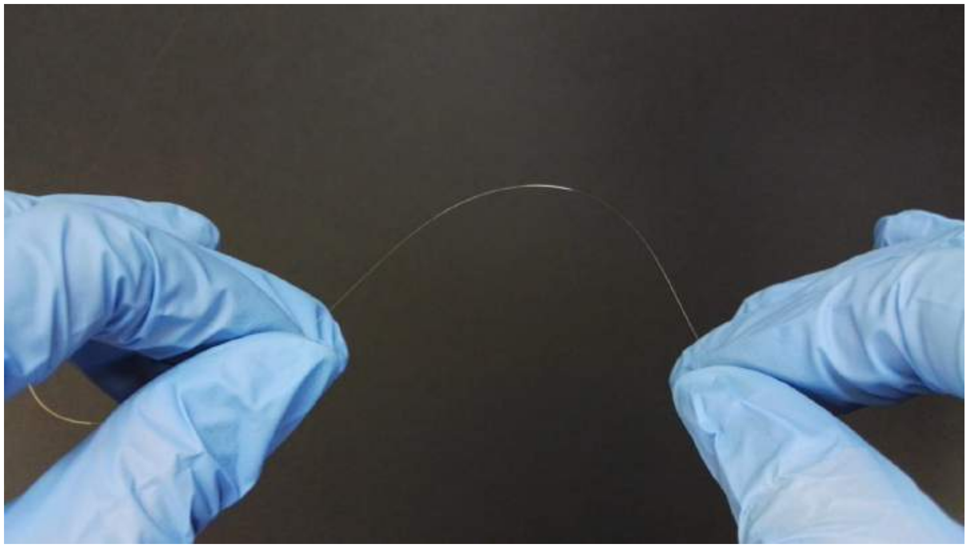

Figure 5.10 - A picture of the welding between a commercial fiber and a phosphate fiber

The picture 5.10 exposes how the mechanical properties of the interface between the different materials are excellent, and allow curvatures with a radius even of the order of 1cm. The welding is at the greatest curvature point.

Conclusions

The whole thesis project had set, as an original objective, the development and production of an innovative phosphate-based glass composition for an optical amplification application, in the perspective of the CALIBER project. About this, it was formulated and developed a phosphate glass system, co-doped with Er^{3+} and Yb^{3+}.
This system was deemed more appropriate for the presence of a high absorption peak of ytterbium ions at 980nm, a wavelength for which high power lasers exist that could act as power pumps, and of the presence of a emission peak of erbium ions at 1550nm, an eye-safe wavelength. Moreover, inside a phosphate glass the transfer of energy from one ion to another takes place with considerable efficiency. Furthermore, using a phosphate-based glass as host glass allows, thanks to the high solubility of rare earths inside it, to increase the concentration of active ions, thus producing theoretically more compact devices.
In order to evaluate the variation of the optical properties for different rare-earth concentrations, three glasses with identical composition, except in the concentration ratio of the active ions, were produced.
Using the glass composition YE1 for the core, and one of the developed cladding glass compositions for the cladding with a targeted Numerical Aperture (NA) of 0.11, a multi-mode optical fiber was realized by preform drawing, with the fiber preform being obtained by the rod-in-tube technique. The fabricated fiber was found free of bubble and major defects.
Guiding properties were verified by near field measurements, confirming that the ligth was well guided inside the core. The measured attenuation coefficient was 3.6dB/m, that is in line with the literature values for phoshate glass fibers.
A setup for CW cladding pump amplification measurements of the realized fiber was designed, developed and characterized. No amplification was detected during these measurements, probably due to imperfect alignment between the optical elements forming the amplification set-up. About this, in order to reduce misalignment losses, the realization of splicing modes to weld together phosphate glass-based fibers and silica glass-based fibers, thus to avoid lossy and time-spending inefficient air alignments, was carried on. The set-up investigation and the implemented recipes can be recommended for further future researches, that could carry out similair

studies towards performing results .

Bibliography

[1] https://caliber-project.eu.

[2] https://www.terabee.com/time-of-flight-principle.

[3] https://www.yellowscan-lidar.com/applications-and-users/how-lidar-works.

[4] https://cutt.ly/deNW7vX.

[5] Gordon Petrie and Charles K Toth. Airborne and spaceborne laser profilers and scanners. In *Topographic laser ranging and scanning*, pages 89–157. CRC Press, 2018.

[6] Nicholas R Goodwin, Nicholas C Coops, and Darius S Culvenor. Assessment of forest structure with airborne lidar and the effects of platform altitude. *Remote Sensing of Environment*, 103(2):140–152, 2006.

[7] Amar Nayegandhi. Lidar technology overview. *US Geological Survey*, 2007.

[8] Fintan Corrigan. 12 top lidar sensors for uavs, lidar drones and so many great uses. DroneZon, 2019.

[9] Rüdiger Paschotta et al. *Encyclopedia of laser physics and technology*, volume 1. Wiley Online Library, 2008.

[10] Ondřej Novák, Taisuke Miura, Martin Smrž, Michal Chyla, Siva Sankar Nagisetty, Jiří Mužík, Jens Linnemann, Hana Turčičová, Venkatesan Jambunathan, Ondřej Slezák, et al. Status of the high average power diode-pumped solid state laser development at hilase. *Applied Sciences*, 5(4):637–665, 2015.

[11] https://fiberlabs.com.

[12] Yusuf Panbiharwala. *Investigation of power scaling issues in pulsed fiber amplifiers*. PhD thesis, 03 2014.

[13] Mircea Guina Davide Janner Daniel Milanese Diego Pugliese Antti Penttinen Antti Harkonen Omri Moschovits Yair Alon Federico Leone Nadia G. Boetti, Amiel Ishaaya. The caliber project. 2019.

[14] Masayuki Yamane and Yoshiyuki Asahara. *Glasses for photonics*. Cambridge University Press, 2000.

[15] https://cutt.ly/ueNQYUf.

[16] MJ Weber. Science and technology of laser glass. *Journal of Non-Crystalline Solids*, 123(1-3):208–222, 1990.

[17] https://www.meta-laser.com/laserglass/erbium-doped-phosphate-glasses.html.

[18] Gerardo Cristian Scarpignato. *Conception, fabrication et caractérisation d'un amplificateur de puissance à base de verres spéciaux pour les sources LIDAR*. PhD thesis, Grenoble, 2014.

[19] Emmanuel Desurvire and Michael N Zervas. Erbium-doped fiber amplifiers: principles and applications. *Physics Today*, 48:56, 1995.

[20] Long Zhang, Hefang Hu, Changhong Qi, and Fengying Lin. Spectroscopic properties and energy transfer in yb3+/er3+-doped phosphate glasses. *Optical materials*, 17(3):371–377, 2001.

[21] https://commons.wikimedia.org/wiki/File:Snells-law.svg.

[22] Safa O Kasap. Optoelectronics. *The Optics Encyclopedia: Basic Foundations and Practical Applications*, 2007.

[23] https://slideplayer.it/slide/2313908/.

[24] Gerd Keiser. Optical fiber communications. *Wiley Encyclopedia of Telecommunications*, 2003.

[25] John A Buck. *Fundamentals of optical fibers*. John Wiley & Sons, 2004.

[26] https://openstax.org/books/college-physics-ap-courses/pages/26-4-microscopes.

[27] Xunsi Wang, Qiuhua Nie, Tiefeng Xu, and Liren Liu. A review of the fabrication of optic fiber. In *ICO20: Optical Design and Fabrication*, volume 6034, page 60341D. International Society for Optics and Photonics, 2006.

[28] Suzanne R Nagel, John B MacChesney, and Kenneth L Walker. An overview of the modified chemical vapor deposition (mcvd) process and performance. *IEEE Transactions on Microwave Theory and Techniques*, 30(4):305–322, 1982.

[29] Than Singh Saini, Nguyen Phuoc Trung Hoa, Tong Hoang Tuan, Xing Luo, Takenobu Suzuki, and Yasutake Ohishi. Tapered tellurite step-index optical fiber for coherent near-to-mid-ir supercontinuum generation: experiment and modeling. *Applied optics*, 58(2):415–421, 2019.

[30] https://www.intechopen.com/books/current-developments-in-optical-fiber-technology/step-index-pmma-fibers-and-their-applications.

[31] https://www.aflhyperscale.com/single-mode-and-multimode-fiber.

[32] https://www.technobyte.org/types-of-optical-fibers-structure-of-optical-fibers/.

[33] Michalis Zervas. High power ytterbium-doped fiber lasers - fundamentals and applications. *International Journal of Modern Physics B*, 28, 04 2014.

[34] PRIYA Murugasen, SURESH Sagadevan, and DEEPA Shajan. Preparation, techniques and tools used for investigating glasses: an overview. *Int. J. Chem. Sci*, 13:695, 2015.

[35] Williams Ebhota, Akhil S Karun, and F. Inambao. Centrifugal casting technique baseline knowledge, applications, and processing parameters: Overview. *International Journal of Materials Research*, 107, 08 2016.

[36] Hirak Naik, Misal Gandhi, Milan Patel, and Rikesh Prajapati. Effect of centrifugal force and speed in casting of aluminium alloy – a review, 09 2018.

[37] http://www.sorame.it/it/produzione/processi-produttivi/colata-centrifuga/.

[38] S Roy Choudhury and Y Jaluria. Practical aspects in the drawing of an optical fiber. *Journal of materials research*, 13(2):483–493, 1998.

[39] https://ioptic.wordpress.com/2011/01/12/cut-back-method-for-testing-fibre-loss/.

[40] Stewart Miller. *Optical fiber telecommunications*. Elsevier, 2012.

Acknowledgements

(Italian)

Ringrazio i miei relatori i professori Davide Janner e Daniel Milanese, ringrazio in particolare la mia corelatrice la dottoressa Nadia Boetti per avermi affiancato con vero supporto durante tutto il mio lavoro di tesi.

Ringrazio la mia famiglia, i miei amici più recenti e di sempre.

Non sarò prolisso, (come al solito). Molti di voi non leggeranno queste pagine, e a loro non potrà arrivare la mia gratitudine per avermi aiutato, in un modo tutto loro, a raggiungere questo traguardo, che non sarà mai solo mio. Ringrazio tutti voi che mi avete supportato e sopportato. Scrivendo i ringraziamenti su questa pagina prometto a me stesso di esprimervi gratitudine il più presto possibile.

Grazie di cuore a tutti, un abbraccio.